

# Global Biogeochemical Cycles®



## RESEARCH ARTICLE

10.1029/2021GB007216

### Special Section:

The Arctic: An AGU Joint Special Collection

## Quantifying Northern High Latitude Gross Primary Productivity (GPP) Using Carbonyl Sulfide (OCS)

Le Kuai<sup>1</sup> , Nicholas C. Parazoo<sup>1</sup> , Mingjie Shi<sup>2</sup>, Charles E. Miller<sup>1</sup> , Ian Baker<sup>3</sup> , Anthony A. Bloom<sup>1</sup> , Kevin Bowman<sup>1</sup> , Meemong Lee<sup>1</sup> , Zhao-Cheng Zeng<sup>4</sup> , Roisin Commane<sup>5</sup> , Stephen A. Montzka<sup>6</sup> , Joe Berry<sup>7</sup>, Colm Sweeney<sup>6</sup> , John B. Miller<sup>6</sup>, and Yuk L. Yung<sup>1,8</sup>

### Key Points:

- Carbonyl sulfide is shown an useful proxy to constrain gross primary productivity in regional and global scales
- This study used Carbon in Arctic Reservoirs Vulnerability Experiment observations and GEOSCHEM modeling of carbonyl sulfide to benchmark the multi-model gross primary productivity at northern high latitude

### Correspondence to:

L. Kuai,  
[le.kuai@jpl.nasa.gov](mailto:le.kuai@jpl.nasa.gov)

### Citation:

Kuai, L., Parazoo, N. C., Shi, M., Miller, C. E., Baker, I., Bloom, A. A., et al. (2022). Quantifying northern high latitude gross primary productivity (GPP) using carbonyl sulfide (OCS). *Global Biogeochemical Cycles*, 36, e2021GB007216. <https://doi.org/10.1029/2021GB007216>

Received 14 OCT 2021

Accepted 8 AUG 2022

### Author Contributions:

**Conceptualization:** Le Kuai, Nicholas C. Parazoo, Charles E. Miller  
**Data curation:** Charles E. Miller, Ian Baker, Anthony A. Bloom, Zhao-Cheng Zeng, Stephen A. Montzka, Joe Berry, Colm Sweeney, John B. Miller  
**Formal analysis:** Le Kuai

© 2022 Jet Propulsion Laboratory, California Institute of Technology. Government sponsorship acknowledged. This article has been contributed to by U.S. Government employees and their work is in the public domain in the USA. This is an open access article under the terms of the [Creative Commons Attribution-NonCommercial-NoDerivs License](https://creativecommons.org/licenses/by/4.0/), which permits use and distribution in any medium, provided the original work is properly cited, the use is non-commercial and no modifications or adaptations are made.

<sup>1</sup>Jet Propulsion Laboratory, California Institute of Technology, Pasadena, CA, USA, <sup>2</sup>Pacific Northwest National Laboratory, Richland, WA, USA, <sup>3</sup>Colorado State University, Fort Collins, CO, USA, <sup>4</sup>University of California Los Angeles, JIFRESSE, Los Angeles, CA, USA, <sup>5</sup>Lamont-Doherty Earth Observatory at Columbia University, Palisades, NY, USA, <sup>6</sup>NOAA Global Monitoring Laboratory, Boulder, CO, USA, <sup>7</sup>Stanford University, Stanford, CA, USA, <sup>8</sup>California Institute of Technology, Pasadena, CA, USA

**Abstract** The northern high latitude (NHL, 40°N to 90°N) is where the second peak region of gross primary productivity (GPP) other than the tropics. The summer NHL GPP is about 80% of the tropical peak, but both regions are still highly uncertain (Norton et al. 2019, <https://doi.org/10.5194/bg-16-3069-2019>). Carbonyl sulfide (OCS) provides an important proxy for photosynthetic carbon uptake. Here we optimize the OCS plant uptake fluxes across the NHL by fitting atmospheric concentration simulation with the GEOS-CHEM global transport model to the aircraft profiles acquired over Alaska during NASA's Carbon in Arctic Reservoirs Vulnerability Experiment (2012–2015). We use the empirical biome-specific linear relationship between OCS plant uptake flux and GPP to derive the six plant uptake OCS fluxes from different GPP data. Such GPP-based fluxes are used to drive the concentration simulations. We evaluate the simulations against the independent observations at two ground sites of Alaska. The optimized OCS fluxes suggest the NHL plant uptake OCS flux of  $-247 \text{ Gg S year}^{-1}$ , about 25% stronger than the ensemble mean of the six GPP-based OCS fluxes. GPP-based OCS fluxes systematically underestimate the peak growing season across the NHL, while a subset of models predict early start of season in Alaska, consistent with previous studies of net ecosystem exchange. The OCS optimized GPP of  $34 \text{ PgC yr}^{-1}$  for NHL is also about 25% more than the ensembles mean from six GPP data. Further work is needed to fully understand the environmental and biotic drivers and quantify their rate of photosynthetic carbon uptake in Arctic ecosystems.

## 1. Introduction

Climate change is fundamentally transforming the Arctic system (Hinzman et al., 2013). These changes have particularly impacted northern high latitude (NHL, 40°N–90°N) terrestrial ecosystems and their associated carbon cycle dynamics. Widespread Arctic greening (Keenan & Riley, 2018; Myers-Smith et al., 2020) and shrub encroachment into tundra ecosystems (Lorant & Goetz, 2012; Myers-Smith et al., 2011) are attributed to accelerated warming and imply increasing NHL photosynthetic carbon uptake (also known as gross primary productivity, GPP). The last 50 years have witnessed a 50% amplification of the NHL CO<sub>2</sub> seasonal cycle (Graven et al., 2013; Jeong et al., 2018) which has been attributed to increased GPP (Forkel et al., 2016; Liu et al., 2020). A key question is whether warming-induced increases in NHL GPP will offset the expected losses in soil carbon due to warming-induced permafrost thaw and respiration (Natali et al., 2019); however, current state of the art models offer no clear consensus on the future trajectory of NHL carbon cycle dynamics (McGuire et al., 2018). Accurate quantification of NHL GPP is therefore critical to help reduce uncertainties in projections of future NHL carbon balance.

The NHL region has a significant impact on global vegetation-atmosphere interactions. Reducing the uncertainty of the carbon uptake in NHL is an essential step for an accurate estimate of the global carbon cycle (Rogers et al., 2021). Absolute values of NHL GPP remain uncertain and there is no solely measurement-based GPP product with which to validate model GPP estimates (Anav et al., 2015). There is general agreement that summertime (June–August) GPP in NHL ecosystems is ~80% of summertime GPP in tropical ecosystems (Norton et al., 2019, Figure 12) and that summertime NHL GPP peaks near 60N, but recent analyses indicate that NHL GPP estimates

**Funding acquisition:** Charles E. Miller, Kevin Bowman  
**Investigation:** Le Kuai  
**Methodology:** Le Kuai, Nicholas C. Parazoo, Mingjie Shi, Kevin Bowman, Meemong Lee  
**Resources:** Le Kuai  
**Supervision:** Charles E. Miller  
**Validation:** Le Kuai  
**Visualization:** Nicholas C. Parazoo  
**Writing – original draft:** Le Kuai  
**Writing – review & editing:** Le Kuai, Nicholas C. Parazoo, Mingjie Shi, Charles E. Miller, Ian Baker, Kevin Bowman, Roisin Commane, Stephen A. Montzka, Joe Berry, Yuk L. Yung

vary by up to 100% (Table 1, estimated from Norton et al., 2019, Figure 12). The spatial distribution of NHL GPP is also highly uncertain, with models varying significantly (Fisher et al., 2014, 2018) and recent analyses emphasizing GPP increases in the boreal forest rather than tundra ecosystems (Byrne et al., 2018; Liu, Kimball, et al., 2020, Liu, Wennberg, et al., 2020). Finally, models struggle to capture seasonal changes in NHL GPP in response to climate change (Forkel et al., 2016). Reliable observational constraints of NHL GPP are therefore imperative for understanding the changing carbon dynamics of the Arctic.

New global ecology observations from airborne and spaceborne sensors allow estimation of gross and net carbon fluxes at regional and global scales (Schimel & Schneider, 2019). These observational constraints are critically needed to reduce carbon cycle uncertainties, especially in the Arctic where models are uncertain and ground observations are still sparse (Schimel et al., 2015). Remote sensing measurements of solar induced chlorophyll fluorescence (SIF) have provided an important proxy for GPP due to the shared relationship with the light reactions of photosynthesis, and the surprisingly invariant linear relationship between spaceborne SIF and eddy covariance GPP at flux towers (Sun et al., 2017). This relationship holds promise for using SIF as a snapshot-in-time proxy for GPP at high latitudes, but satellite remote sensing constraints are more complicated in high latitude ecosystems due to smaller vegetation signals, shorter growing seasons and rapid transition seasons, high view and solar angles, infrequent sampling, and single overpass times characteristic of orbital sensors (Parazoo et al., 2021).

Carbonyl sulfide (OCS) is another increasingly important proxy for biogenic activity and GPP (Berry et al., 2013; Campbell et al., 2008), with atmospheric mole fraction measurements complementing remote sensing data by providing spatially and temporally integrated constraints (Whelan et al., 2020). OCS uptake gives a direct measurement of stomatal conductance and this can be related to CO<sub>2</sub> uptake and photosynthetic activity (Berry et al., 2013; Campbell et al., 2008; Commane et al., 2015; Maseyk et al., 2014; Seibt et al., 2010; Wehr et al., 2017), and therefore covaries seasonally with CO<sub>2</sub> (Berry et al., 2013; Montzka et al., 2007; Parazoo et al., 2021; Suntharalingam et al., 2008; Wang et al., 2016).

Long-term atmospheric measurements of OCS from NOAA's Barrow Atmospheric Baseline Observatory (BRW) exhibit an increasing seasonal amplitude trend similar to that observed for CO<sub>2</sub> (Campbell et al., *in press*), supporting previous evidence of accelerated biospheric activity in northern high latitudes over previous decades (Graven et al., 2013; Jeong et al., 2018). The seasonal amplitude of OCS is ~20% of its background level, compared to only 5% for CO<sub>2</sub>, providing a stronger signal of biospheric activity (Montzka et al., 2007). Additionally, the major OCS source comes from the ocean and the dominant OCS sink comes from terrestrial photosynthesis. They are spatially well separated. Table 2 summarizes more comparisons of the global budgets for all the sources and sinks from the previous studies. While the combination of these factors provides increasing promise that the change in OCS mole fraction observed at the towers in Alaska originates from biospheric processes, the challenge remains to isolate Alaskan biospheric activity from long-range transport on measured OCS mole fraction (Barnes et al., 2016; Parazoo et al., 2016).

The value of regular measurements of atmospheric CO<sub>2</sub> and related trace gas vertical profiles in quantifying regional scale carbon fluxes is well established (Sarmiento & Wofsy, 1999; Sweeney et al., 2015). These strategies isolate regional biospheric activity from long-range transport by differencing trace gas mole fractions in the free troposphere (FT) (background values) from those in the boundary layer (BL) (local values) (Commune et al., 2017; Parazoo et al., 2016; Sweeney et al., 2020). There are currently two main strategies for measuring OCS from aircraft within continental interiors: Fixed-point networks versus spatially resolved campaigns. The NOAA/Global Monitoring Laboratory (GML) light aircraft network focuses on year-round, fixed location, high-precision airborne flask measurements at multiple altitudes from the surface up to 8 km above sea level, and multiple locations across North America (Montzka et al., 2007; Sweeney et al., 2020). Network style data are reliable and long-term, and are particularly effective for studying regionally integrated processes at seasonal and longer time scales. For example, vertical OCS profiles from the NOAA/GML network in 2005–2012 indicate a regional hotspot of photosynthetic activity in the Midwest US, providing an important evaluation for studying temporal and spatial patterns in models (Hilton et al., 2017).

Intensive airborne campaigns, on the other hand, typically focus on long-distance transect flights to sample multiple air masses across biologically diverse regions, sometimes multiple times per day, at spatial scales ranging from 100 to 1,000 km. Moreover, airborne campaigns that fly into and out of the atmospheric boundary layer

**Table 1**  
*Model Estimates of Summertime (June–August) Northern High Latitude Gross Primary Productivity*

Analysis	60N GPP (gC m <sup>-2</sup> d <sup>-1</sup> )	NHL GPP range (40–70N)(gC m <sup>-2</sup> d <sup>-1</sup> )
FLUXCOM GPP	5.0	1.5–5.0
TRENDY mean	6.0	2.0–6.0
TRENDY 10th percentile	5.0	1.5–5.0
TRENDY 90th percentile	8.0	3.0–8.0
BETHY-SCOPE	9.0	2.0–9.0

(BL) can sample air immediately in contact with the surface for increased sensitivity to local processes, as well as provide a periodic sampling of background air in the FT, thus accounting for the influence of long-range transport (Baier et al., 2020; Parazoo et al., 2016). For example, the Atmospheric Carbon Transport (ACT)—America campaign from 2016 to 2019 collected flask profiles of OCS and other trace gases across biologically diverse regions in the eastern US, filling spatial gaps left by tower and airborne networks, and providing novel evidence of late season photosynthetic uptake in humid temperate forests in the southern US that is unaccounted for in models (Parazoo et al., 2021).

In this paper, we exploit airborne observations of OCS from the Carbon in Arctic Reservoirs Vulnerability Experiment (CARVE, Miller et al., 2012) to study plant driven carbon uptake in Alaska. CARVE observations of CO<sub>2</sub>

and CH<sub>4</sub> have previously been used to study seasonal and interannual changes in net biome exchange (NBE) and methane emissions across Alaska (Commane et al., 2017; Parazoo et al., 2018; Zona et al., 2016). This study leverages CARVE OCS data to gain additional insights into NHL GPP. Our main objective is to use data constrained estimates of OCS uptake in Alaska to evaluate model estimates of photosynthetic carbon uptake, and then use our optimized model to estimate seasonal photosynthetic carbon uptake across the NHL. To this end, we use an optimized OCS simulation with the GEOS-CHEM global transport model to fit aircraft vertical profiles of OCS measured over Alaska during the CARVE campaign (2012–2016) for optimized estimates OCS fluxes across the NHL (40°N to 90°N).

Many biosphere models use a Leaf Relative Uptake (LRU) scaling factor to relate OCS uptake and GPP on a leaf scale (e.g., Hilton et al., 2017). A commonly used value is ~1.6, although distribution of LRU values has been observed (Whelan et al., 2018). The Simple Biosphere Model (SiB3; Baker et al., 2003; Baker et al., 2008; Parazoo et al., 2020) calculates OCS uptake based on leaf physiology and soil properties (Berry et al., 2013), and has been evaluated against a variety of observational data (Commane et al., 2015; Glatthor et al., 2015; Hilton et al., 2017; Hu et al., 2021; Kooijmans et al., 2021; Kuai et al., 2015; Villalba et al., 2021; Wang et al., 2016). Similarly to LRU but on an ecosystem scale, we derived linear regression models for each biome from SiB3 GPP and SiB3 to calculate OCS plant uptake flux. We applied the linear models based on biome types to an ensemble of other GPP models, which allow us to introduce a framework of using OCS measurements to evaluate a

**Table 2**  
*Global Budget Estimation of Carbonyl Sulfide Sources and Sinks From Previous Studies (Units: Gg S/yr)*

Sources	Kettle et al., 2002	Berry et al. (2013)	Kuai et al. (2015)	This study	Lennartz et al. (2021)
Direct OCS from Ocean	39	39	41	26	110
Indirect OCS as DMS from Ocean	81	81	83	54	
Indirect OCS as CS <sub>2</sub> from Ocean	156	156	155	100	175
Direct Anthro	64	64	62	295	
Indirect Anthro as CS <sub>2</sub>	116	116	113		
Indirect Anthro as DMS	0.5	0.5	0		
Biomass Burning	11	136	49	102	60 ± 37 Stinecipher et al. (2019)
Missing Photochemical Ocean Source	0	600	559	588	
TOTAL SOURCES	467.5	1192.5	1062	1165	
SINKS	Kettle et al. (2002)	Berry et al. (2013)	Kuai et al. (2015)	This study	
OH Radical	−94	−101	−111	−111	
Plant Uptake	−238	−738	−755	−875	
Soil Uptake	−130	−355	−176	−176	
TOTAL SINKS	−462	−1194	−1062	−1162	
Net	5.5	−1.5	0	3	

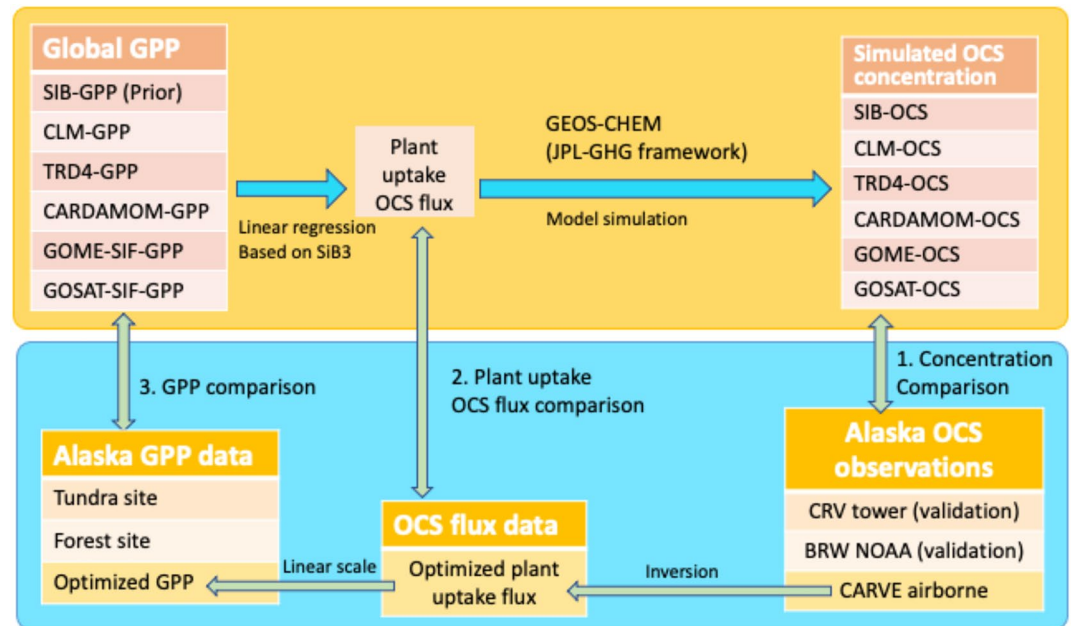


**Figure 1.** The flowchart for this study to improving gross primary productivity budgets with Carbonyl sulfide (OCS). The version of the GEOS-CHEM is developed at JPL for multi-greenhouse gases including CO<sub>2</sub>, CO, CH<sub>4</sub> in addition to OCS. TRD4 stands for TRENDY-v4 (dynamic global vegetable model project). The locations for CRV tower, BRW National Oceanic and Atmospheric Administration, forest and tundra sites are showed in Figure 2.

multi-model GPP data set from distinct sources, using Alaska as a case study. This method is potentially applicable to a global scale study using satellite observations such as TES (Kuai et al., 2014) and MIPAS (Glatthor et al., 2015, 2017), or combining aircraft campaigns globally including HIPPO, ATOM, and NOAA aircraft campaigns over N. America.

## 2. Methods

The flow chart in Figure 1 illustrates the framework we used in this study. It focuses on optimizing and evaluating models against eddy covariance flux data (GPP and OCS plant uptake) and atmospheric mole fraction data (OCS). Surface flux and mole fraction data are described in Section 2.1 and summarized in Tables 2 and 3. First, we acquire GPP estimates from different model sources (Section 2.2), then convert from GPP to OCS plant uptake flux using a linear scaling relationship derived from predictions of GPP and OCS plant uptake in the SIB3 diagnostic model (Section 2.3). Next, we use the GEOS-Chem atmospheric transport model as an observation operator to compare modeled OCS to observed OCS mole fractions (Section 2.4). We then derive CARVE optimized fluxes of OCS through minimizing the difference between the predicted and observed mole fractions

**Table 3**  
*Summary of Observation Data and Their Applications in This Study*

Observations	OCS concentration	GPP flux	Period	Model comparison
CARVE campaign	Regional profiles	_____	2012–2016 April–November	Regional scale; Vertical gradient; Seasonal variation
NOAA BRW site	Surface record	_____	2000–2016	Local scale; Long-term trend; Seasonal variation
CRV tower site	Surface record	_____	2012–2016	Local scale; Short-term trend; seasonal variation
Tundra site	_____	Tower data	2008–2016	Local scale; Seasonal variation
Forest site	_____	Tower data	2008–2016	Local scale; Seasonal variation

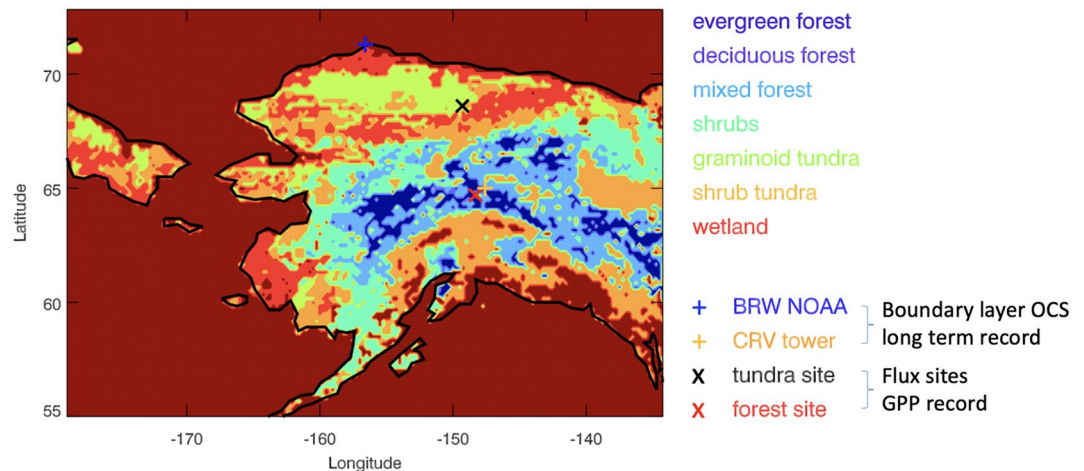


**Figure 2.** Complex vegetation coverage at Arctic Alaska. Two ground sites for Carbonyl sulfide concentration observations (BRW site by National Oceanic and Atmospheric Administration and CRV tower site). Two flux tower sites for gross primary productivity (tundra site and forest site).

(Section 2.5). We furthermore derive optimized GPP fluxes by scaling model GPP as the ratio of optimized to model OCS fluxes (Section 2.6).

## 2.1. Flux Tower and Atmospheric Data

### 2.1.1. Eddy Covariance Derived GPP Flux

We examine two flux tower sites in Alaska that provide partitioned GPP data over forest and tundra (Figure 2). The in situ NEE measurement is partitioned into GPP and ecosystem respiration by using the sensitivity of ecosystem respiration to temperature from night time to day time (Reichstein et al., 2005). The night-time measurements of NEE indicates night-time respiration, which can further be used to derive the day-time respiration by considering the temperature sensitivity of ecosystem respiration. Thus, day-time measured NEE and estimated day-time ecosystem respiration can be applied to partition GPP. We analyze clusters of three towers each for the tundra and interior forest regions. The tundra towers are located at the Innavait Creek watershed in the northern foothills of the Brooks Range in northern Alaska (Euskirchen et al., 2017). The forest towers are located at the Bonanza Creek Long-Term Ecological Research station (<https://lternet.edu/site/bonanza-creek-lter/>) in a boreal peatland lowland of the Tanana Flats, ~30 km southeast of Fairbanks (Euskirchen et al., 2014). All three forest towers are located within 0.5 km of each other. Data were collected from each of the six towers from 2008 to 2016 and partitioned into GPP and TER components using the relation between NBP during the nighttime ( $PAR < 50 \text{ } \mu\text{mol/m}^2/\text{s}$ ) and air temperature (Euskirchen et al., 2017; Reichstein et al., 2005). These datasets were used in a previous model GPP evaluation in Alaska (e.g., Parazoo et al., 2018). For this analysis, we create across-tower monthly averages for the tundra and forest clusters (leaving two monthly time series for each site), then produce climatological seasonal cycles using multi-year monthly averages from 2008 to 2016 (leaving 12 monthly data points at each site).

### 2.1.2. Tower OCS Measurements

Another tower-based measurements of atmospheric trace gas mole fraction (“mole fractions”) of OCS are taken from the CARVE tower (CRV;  $-147.6^\circ\text{E}$ ,  $65.0^\circ\text{N}$ , 643.1 m ASL; Figure 2) in Fox, Alaska from 2012 to 2016 as part of the EV-S1 CARVE investigation (Karion et al., 2016). The CRV tower location was chosen for its high elevation compared to the immediate surrounding mean ground level and its relatively large region of influence in interior Alaska. CRV OCS data were derived from NOAA’s Global Monitoring Laboratory (NOAA/GML) measurements of whole air samples collected by a Programmable Flask Package (PFP) from the top of the tower at 32 m agl (Miller et al., 2016; Montzka et al., 2007). Flasks were collected daily from April to October and weekly from November to March each year. This resolved the seasonal OCS uptake dynamics in fine detail as well as provided accurate coverage of the shoulder seasons and cold season atmospheric OCS mole fractions. The

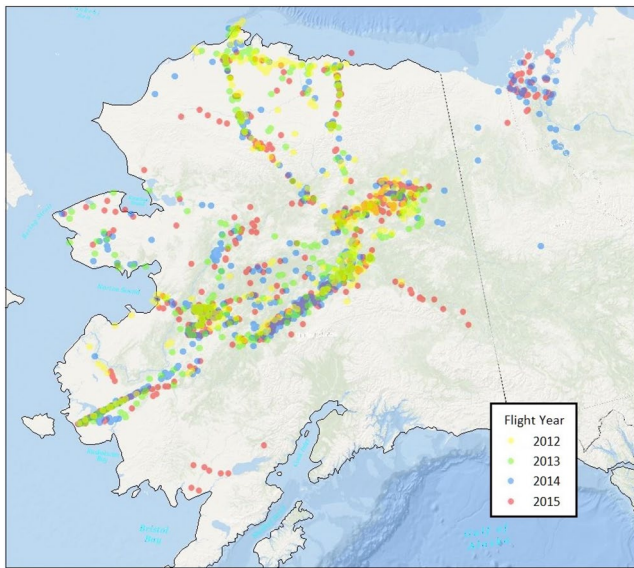


**Figure 3.** A map illustrating the locations and years in which the CARVE airborne Programmable Flask Package samples were acquired. The Carbonyl sulfide mole fractions from these measurements sample across Alaska's Arctic and boreal ecosystems as well as across four different growing seasons (Sweeney et al., 2016).

CRV data provided a quasi-continuous time series data record with which to contextualize the periodic CARVE airborne OCS measurements.

We also use long-term flask measurements from the Barrow tower (BRW;  $-156.6^{\circ}\text{E}$ ,  $71.3^{\circ}\text{N}$ , 11 m ASL) along the northern coast of Alaska from 2004 to 2016 (see Figure 2). These data are collected and analyzed by NOAA/GML, which has provided a reliable source of validation data for models and studies of both seasonal variability and global budgets (Montzka et al., 2007). The NOAA measurements include 12 individual sites over the world taking flask sampling data approximately weekly at most sites since 2000.

### 2.1.3. Airborne OCS Measurements

CARVE flights occurred monthly from April to November (roughly DOY 100–300) from 2012 to 2016 during which PFP samples were collected in the BL ( $>900$  hPa) and FT (700–400 hPa) across the Arctic and boreal Alaska (Figure 3), and later analyzed at NOAA/GML for OCS and other GHGs (Miller et al., 2016). CARVE flights covered the growing season (DOY 150–240) in all years, with later years increasingly focused on the spring/fall transition seasons. Airborne profile measurements provide vertical, horizontal, and temporal information.

## 2.2. Model GPP Estimates

We leverage a range of GPP estimates from two process models (SIB3, CLM), the TRENDY model intercomparison project, and three model-data fusion systems (CARDAMOM, GOPT-GOME2, GOPT-GOSAT). We carefully choose them because they estimate GPP with the three different mechanisms mentioned above. The diversity of such selection could represent a reasonable range of the GPP uncertainties.

The Simple Biosphere Model version 3 (SIB3) involves the use of explicit biophysical mechanisms to directly calculate carbon assimilation by photosynthesis, and prognostic calculations of canopy air space and structural properties (Baker et al., 2003, 2008) and has been updated to calculate OCS as discussed in Section 2.3. The Community Land Model (CLM) version 4.5 includes a full representation of plant biogeochemistry and prognostic carbon dynamics (Oleson et al., 2013). We also include model ensemble averages from version 4 of the TRENDY (TRD4) model intercomparison project (<http://dgvn.ceh.ac.uk>) (Sitch et al., 2015), which only includes prognostic models.

We used the version of CARBON Data Assimilation Model Framework (CARDAMOM; Bloom et al., 2016) GPP that only applied the GOME-2 relative variability but the GPP magnitude is from FLUXCOM mean values. For the GPP derived from satellite observed SIF data, we leverage the CARBON Data Assimilation Model Framework (CARDAMOM; Bloom et al., 2016), which provides spatially explicit optimization of terrestrial carbon cycle models using a simplified modeling framework constrained by diverse satellite remote sensing observations. We also use a Bayesian analysis framework to estimate monthly average GPP that optimally accounts for uncertainties in predictions of GPP from terrestrial biosphere models, estimates of GPP inferred from satellite observations of SIF, and biome specific linear relationships between SIF and upscaled flux tower GPP from FLUXCOM (Parazoo et al., 2014). We use level 2 ungridded SIF data from two separate instruments to constrain the TRD4 ensemble, including the Greenhouse Gases Observing SATellite (GOSAT), which has small footprints ( $\sim 10$  km diameter) at midday ( $\sim 1:30$  p.m.) but sparse data collection, and the Global Ozone Monitoring Instrument onboard Metop-A (GOME2), which has coarse footprints ( $\sim 40 \times 80$  km<sup>2</sup> prior to 15 July 2013 and  $40 \times 40$  km<sup>2</sup> afterward) from mid to late morning ( $\sim 9:30$  a.m.–noon; e.g., Joiner et al., 2020) but nearly continuous spatial mapping. SIF is retrieved following Frankenberg et al. (2011) for GOSAT, and following Kohler et al. (2015) for GOME2. In the following discussion, we will use SIB, CLM, GOSAT, GOME, TRD4, and CARDAMOM to refer to the above GPP models we studied.

### 2.3. Estimating OCS Fluxes From GPP Models

It is challenging to validate model GPP due to our limited ability to directly measure GPP at the canopy and ecosystem scales (Baldocchi et al., 2018). Multiple empirical estimates are available, which make use of vegetation optical remote sensing, but these require models and/or ancillary information to predict GPP from absorbed, reflected, or emitted light. Current best estimates of ecosystem GPP use Eddy covariance (EC) tower fluxes and remotely sensed land cover maps in a machine learning framework to upscale GPP estimates from the site level to landscape and regional scales; however, these estimates require partitioning methods relying either on light response curves (Lasslop et al., 2010), artificial neural networks (Papale et al., 2006), and/or models of temperature sensitivity (Reichstein et al., 2005), which are highly uncertain. Reliable tower measurements are increasingly available throughout the Arctic and sub-Arctic, but represent very different spatial scales and environments compared to most models (Ueyama et al., 2013).

Plant uptake of atmospheric CO<sub>2</sub> and OCS are directly related to photosynthesis through diffusion by stomatal conductance and consumption by collocated reaction in the chloroplasts of leaves (Rubisco and carbonic anhydrase (CA), respectively) (Berry et al., 2013; Campbell et al., 2008). As such, atmospheric OCS observations provide an opportunity to more directly evaluate the model estimates of GPP at multiple temporal and spatial scales. However, even though most terrestrial biosphere models include a representation of stomatal conductance, most models don't simulate leaf-level OCS uptake. To circumvent this limitation, we developed a simplified biome specified linear regression method that converts the GPP into the OCS plant uptake globally from the mechanism in the SIB model. Diffusion of gases including CO<sub>2</sub>, OCS, and water vapor along the pathway from the atmosphere to the leaf cell where biochemistry takes place is controlled by boundary layer, stomatal, and mesophyll conductance (Berry et al., 2013). The prognostic canopy air space in SIB, and the addition of mesophyll conductance scaling to V<sub>cmax</sub> (and modulation by environmental conditions), enable direct calculation of plant OCS uptake (Baker et al., 2003; Stockli & Vidale, 2005).

Analysis of monthly mean plant uptake of OCS and GPP output from SIB shows a biome-dependent linear relationship (Figure A1). Therefore, we compute the linear regressions from GPP to OCS flux for the regional ecosystems. We compute the slope “*k*” and interception “*b*” in Equation 1 using SIB's GPP ( $F_{GPP}$ ) and OCS plant uptake ( $F_{OCS}$ ) data for each biome.

$$F_{OCS}(x, y) = k(ib) \times F_{GPP}(x, y) + b(ib) \quad (1)$$

where “(x,y)” represents the index for latitude and longitude. “*ib*” is the index for the biome type.

By applying the consistent biome specified regression model, we derive OCS plant uptake from any other GPP data set. We hereafter refer to estimates of OCS using the linear regression model as “model OCS flux.”

### 2.4. Atmospheric OCS Mole Fraction Simulations

While we focus on OCS uptake by Alaskan ecosystems, we must account for all ocean, terrestrial, and anthropogenic OCS fluxes and be able to convert these fluxes into accurate estimates of atmospheric OCS mole fractions to compare simulated against measured values. GEOS-CHEM is a well-established atmospheric transport modeling system and has been used previously for global OCS analyses (Kuai et al., 2015; Suntharalingam et al., 2008; Wang et al., 2016). Recently, Sweeney et al. (2020) demonstrated that GEOS-CHEM provided accurate atmospheric transport for regional studies of atmospheric CO<sub>2</sub> focused on Alaska.

In this study, we use GEOS-CHEM to simulate global atmospheric OCS mole fractions at 2° × 2.5° spatial resolution using GEOS-5 reanalysis data, with output analyzed at 3 hr time steps. Model simulations use common emission inventories including global ocean flux (Kettle et al., 2002; Kuai et al., 2015), the soil sinks from SIB (Berry et al., 2013), anthropogenic emission (Campbell et al., 2015) and biomass burning (Kuai et al., 2015). We also implement a common sink due to soil and OH but test different model-based estimates of OCS plant uptake derived from our OCS-GPP linear model. The atmospheric OCS predictions from these tests refer as “model OCS mole fraction.” Unlike CO<sub>2</sub>, which is driven by the imbalance between GPP and respiration, the OCS seasonal signal is driven predominantly by GPP. The magnitude and timing of summer GPP determine the magnitude and timing of the seasonal OCS minimum, which is offset by maximum GPP flux due to the atmospheric transport

**Table 4**

The Global and Regional Integrated Annual Carbonyl Sulfide Flux and Gross Primary Productivity (Green: Low-Value Group; Red: High-Value Group; Blue: Benchmark Value)

GPP version	OCS flux (Gg S yr <sup>-1</sup> )		GPP (PgC yr <sup>-1</sup> )	
	Global	Regional (40°N~90°N)	Global	Regional 40°N~90°N
CARDAMOM	-880	-149	111	23
SIB3	-865	-161	104	21
GOME	-819	-139	95	20
GOSAT	-1024	-220	116	29
CLM	-1062	-241	129	33
TRD4	-1075	-244	146	34
Ensemble	-954	-192	117	27
Optimized	-953	-247	121	34

lag (Parazoo et al., 2016). The onset of the growing season, the timing, and the length of the senescent period all affect OCS seasonality.

### 2.5. CARVE Optimized OCS and Pan-Arctic GPP

We also used GEOS-Chem as a forward model to constrain predicted OCS flux against seasonally resolved CARVE OCS vertical profiles and then evaluated optimized simulation with the observations from CRV and BRW towers. The optimized OCS flux is inverted by fitting the model vertical profiles with the CARVE observed OCS profiles especially over summer seasons. The SIB plant uptake was used as a prior flux and one constant scaling factor was optimized and applied to the prior flux from 60°N to 90°N. This scaling factor was repeatedly used for the year since 2004 to 2016.

### 2.6. Optimized GPP

The optimized posterior OCS flux was used to infer an optimized GPP product at a regional scale. We estimated the annual plant uptake over the region 40°N to 90°N for all GPP-based flux and the optimized flux as well as the annual GPP over the same region (summarized in Table 4). Equation 2 was used to estimate the optimal annual GPP ( $GPP_{opt}$ ) over the region by scaling the GPP ensemble ( $GPP_{ens}$ ) with the ratio of the optimized plant OCS uptake flux ( $F_{opt}$ ) to the ensemble plant OCS uptake flux ( $F_{ens}$ ).

$$GPP_{opt} = \frac{F_{opt}}{F_{ens}} \times GPP_{ens} \quad (2)$$

## 3. Results

Figure 4 shows the temporal variation of the atmospheric OCS mole fraction observed at the CRV site (boreal forest) and at NOAA's BRW site (tundra). We compare the profiles of different modeled atmospheric OCS mole fractions to CARVE airborne data (Figure 5) and the vertical drawdown seasonal variations (Figure 6). Then we evaluate the modeled simulations by comparing the surface model fractions in the long term seasonal variability to the tower observations at CRV and BRW (Figure 7).

With the verification of improved agreements between the optimized OCS mole fractions and the observations from different platforms, we can use the optimized OCS fluxes to infer regional scaled GPP and evaluate both OCS fluxes and GPP we studied here. This study is first summarized in comparisons of all kinds of GPP based OCS plant uptake fluxes to the optimized OCS fluxes across the pan-Arctic, focusing on the Northern Hemisphere mid-latitude to polar region from 40° to 90°N (Figure 8).

Next, we compare the ensemble of GPP seasonality with the observation-based GPP from tower sites at the local scale (Figure 9). At last, we evaluate the GPP datasets with the OCS optimized GPP at the pan-Arctic scale latitudinally and globally (Figures 10 and 11), which cannot be addressed sufficiently with limited tower data.

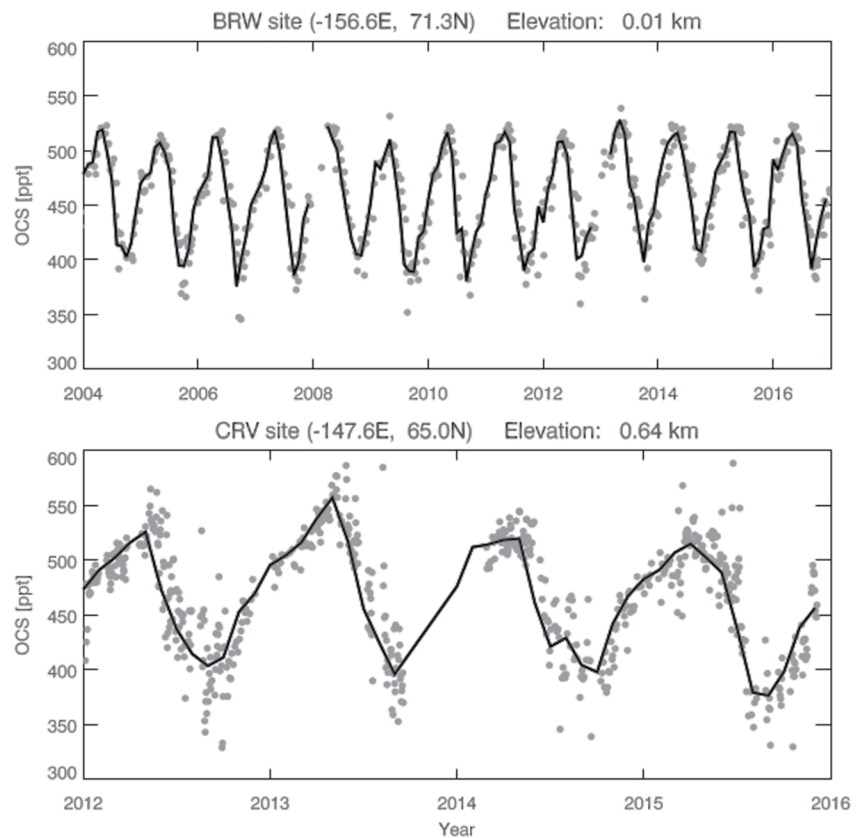


**Figure 4.** Top: The Carbonyl sulfide (OCS) concentration time series from the BRW tower extends from 2004 to the present. Measurements are made twice per month on average. Bottom: The OCS concentration measurements from the CRV tower were recorded daily from April–October and weekly from November–March each year from 2012 to 2015. Gray dots are the raw data. The black line is the monthly mean, which is used for the next model validation. The OCS seasonal cycle in each location varies from ~550 to ~350 ppt each year, with a peak drawdown of more than 35%.

### 3.1. The Comparison of OCS Between Model Simulations and Observations

#### 3.1.1. Simulated OCS Comparison to Aircraft and Tower Data

We show the raw OCS observations (dots in Figure 4) at both BRW site (top) and CRV site (bottom) and overplot the data with their monthly mean time series in the black lines. Measurements have been reported from the BRW site from an inlet 8 m above ground three times per month on average from the year 2000 to the present. There is some inter-annual variability in the amplitude of the seasonal cycle but no obvious trend in the long term record.

The periodical CRV data from 2012 to 2016 were taken more frequently every year from late spring until fall than from winter to early spring. The measurements are recorded daily from April to October and weekly from November to March each year. Raw data vary from ~550 ppt (peak in spring until the growing season starts) to ~350 ppt (in late summer until drawdown ends). The peak to peak difference is more than 35% of the OCS mole fraction.

We compare the OCS monthly mean vertical profiles between model simulations and CARVE airborne measurements in Figure 5. Both model simulations and CARVE airborne OCS measurements are multi-year monthly averaged for the 2012–2016 period. The gray lines represent vertical profiles from the six simulations driven by GPP based OCS plant uptake fluxes plus the Parameterized Chemical Transport Model (PCTM) simulation from Berry et al., 2013. Their ensemble means' vertical profile is shown in black dash line. The forward model simulations have larger variations in boundary layer than in the upper troposphere but show the consistently weaker vertical differences than the CARVE observations, especially when the vertical gradient is large in the summer months. In the boundary layer, the OCS-optimized profile (red dash line below 900 hPa) shows improved

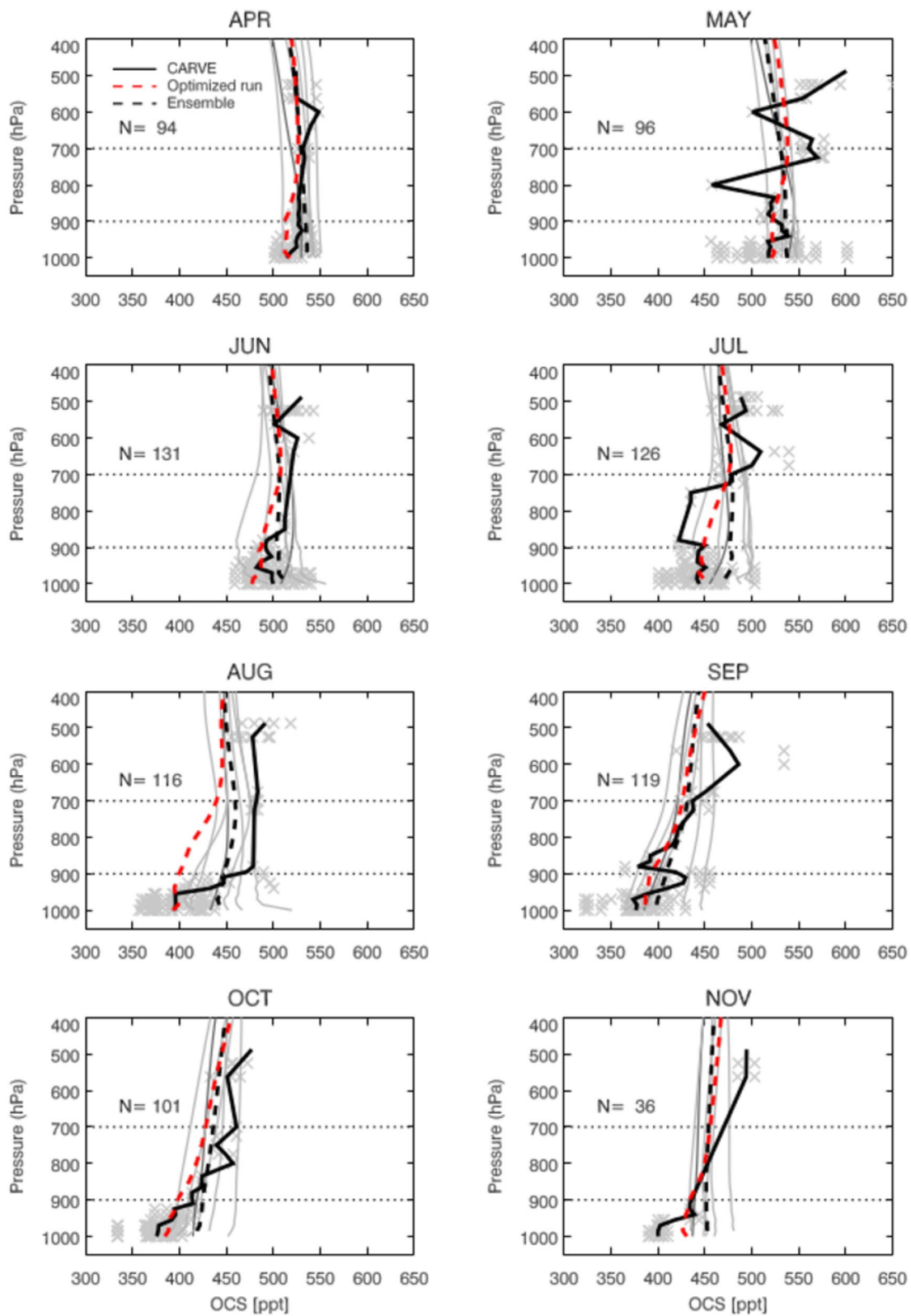
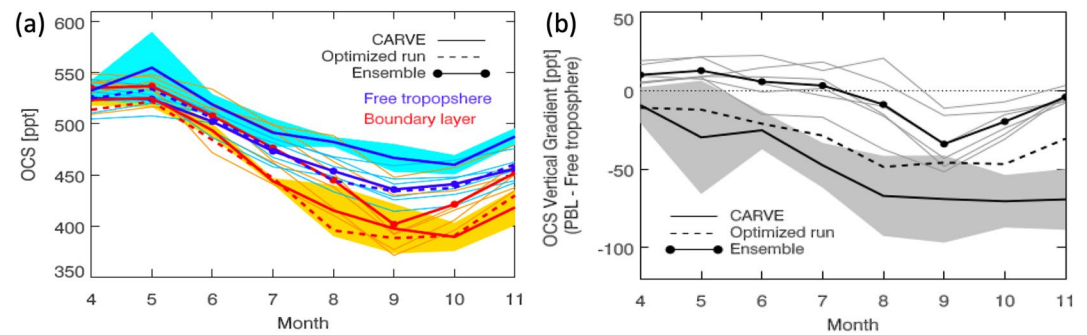


Figure 5.



**Figure 6.** (a) Comparisons of the seasonal variations of Carbonyl Sulfide in the boundary layer (BL, averaging below 900 hPa, plotted in red) and the free troposphere (FT, averaging between 700 and 400 hPa, plotted in blue) between the simulations and Carbon in Arctic Reservoirs Vulnerability Experiment (CARVE) observations. The solid red and blue lines are the mean CARVE values for the BL and FT, respectively while the orange and light blue shaded regions represent one standard deviation about those means. The red and blue dashed lines are our optimized BL and FT simulations. The thin lines are from other simulations and their ensemble means are plotted in lines with diamonds. (b) Comparisons of the vertical gradient (=BL - FT).

agreement with the CARVE observed profiles (black solid line) than the model ensemble profiles in most months, especially during the summer season with strong surface uptake in the boundary layer.

The April CARVE data show a nearly constant vertical profile consistent with minimal photosynthetic activity in the late cold season. The large variability ( $\sim 150$  ppt) of near surface ( $P \sim 1000$  hPa) in CARVE observation is noticed in May because of the start of the growing season in the south (OCS drawdown), while more northerly portions of the domain are still frozen and senescent. Drawdown continues through the June–July–August peak of the growing season, with near surface OCS clustering into values that drop  $\sim 50$  ppt per month from  $500 \pm 50$  ppt in June to  $400 \pm 50$  ppt in August. During this period the free tropospheric OCS mole fractions also decrease, from  $\sim 525 \pm 50$  ppt in June to  $\sim 475 \pm 50$  ppt in August, creating gradients in the vertical profile. The shoulder season months of September and October show increased near surface variability, with measurements below 350 ppt, partially driven by long-range transport from lower latitudes (e.g., Parazoo et al., 2016; Sweeney et al., 2020) while free tropospheric values drop to  $\sim 450 \pm 50$  ppt. Vertical gradients are strongly diminished by November with reduced biological activity.

Compared to the CARVE observations, we find that the vertical drawdown is still too weak in most OCS models, especially in boreal summer. This weak vertical drawdown is also found in SIB based simulations of OCS within an offline Parameterized chemistry transport model (PCTM) similar to GEOS-Chem (Berry et al., 2013). This suggests the discrepancy is common in the simulations from two models with the same plant uptake. However, the optimized run in GEOS-Chem has notably stronger vertical drawdown than above model ensemble runs, in much better agreement with CARVE observations.

The strongest vertical drawdown of the year occurs in August and September, with individual CARVE samples showing depletion in the boundary layer of 50–150 ppt over a vertical depth of 100 hPa from the surface to 900 hPa. The optimized vertical profiles in these months show broad agreement with CARVE profiles, owing to enhanced boundary layer OCS depletion by optimized plant uptake to stronger values in growing and summer seasons. On average, models underestimate plant drawdown during peak summer months, but the model spread is high and there is a subset of models with a strong vertical drawdown in August and September.

We find the low amount of FT OCS is another important reason for the remaining weaker vertical gradients than the CARVE measurements. Since the optimized run only constrains plant uptake which only effectively impacts the surface level, the existing low background level in the FT was not solved in the optimized simulation, leading to remain insufficient enhancement to free tropospheric OCS, especially during June–August. Therefore,

**Figure 5.** The comparisons of the monthly Carbonyl sulfide (OCS) vertical profiles between the optimized and gross primary productivity (GPP)-based simulations and the Carbon in Arctic Reservoirs Vulnerability Experiment (CARVE) observations. Gray crosses mark the CARVE raw data and their averaged profiles are shown in black solid lines. The red dash lines are the optimized profiles. The gray solid lines are the profiles from the GEOS-chem simulations driven by SIB, GOME, GOSAT, CLM, TRD4, or CARDAMOM GPP-based OCS plant uptake fluxes individually and plus one from Parameterized Chemical Transport Model simulation. Their ensemble mean profiles are plotted in black dashed lines.

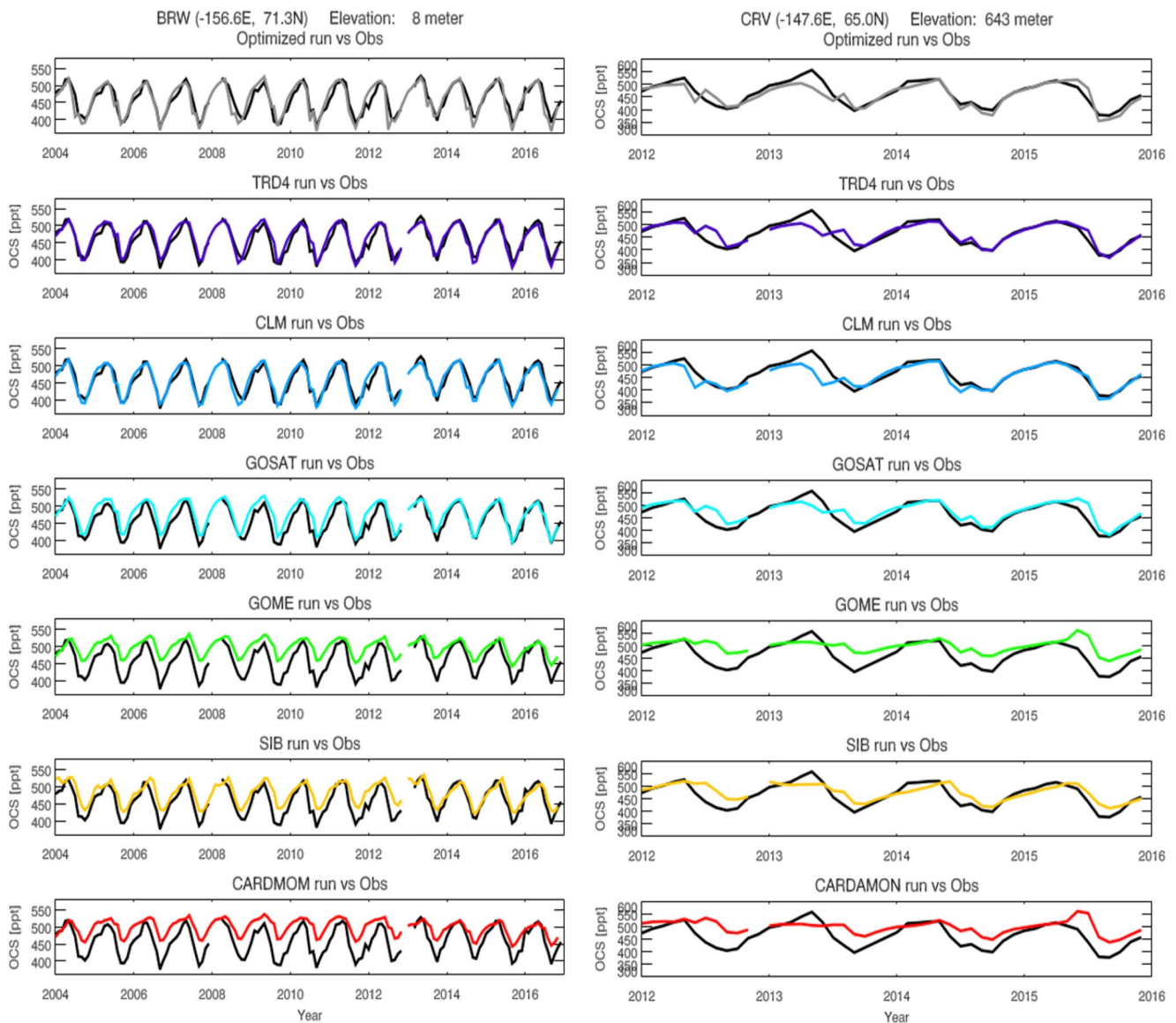


**Figure 7.** The comparisons of the monthly mean time series between the simulations (colored lines for different Carbonyl Sulfide-based Carbonyl Sulfide simulations) and observations (black lines) at BRW site (left column) and CRV site (right column). Note that the black lines in the same column are replicate of the observations at the site. The two black lines for BRW site and CRV site are also the same black lines at two sites shown in Figure 4.

even though the boundary layer is improved in the optimal run, the vertical drawdown remains too weak. The low background level in all model simulations may suggest the need for a stronger ocean source and consequently an enhanced sink for balanced global budget. Our study suggests where the land OCS uptake can be stronger.

We further show the observed and simulated anomalies in the OCS vertical gradient through a comparison of the seasonal variations of the BL (below 900 hPa level), the FT (above 700 hPa level) and their differences in Figure 6. The CARVE observations reveal a gradient of 10–25 ppt in April and May, prior to the growing season onset. The difference increases throughout the growing season, peaking at ~75 ppt from September and October.

Our optimized run agrees with the observed seasonal OCS variability in the BL within  $1\sigma$  of observed variability (Figure 6a). The optimized run systematically underestimates free tropospheric OCS mole fractions by 20–30 ppt, the same as the model ensemble mean. In fact, the optimized run tracks closely with the seasonal variability from the model ensemble mean. The differences between the optimized run and FT measurements are also reflected in the seasonal values of the BL and FT gradient (Figure 6b), where the difference between the

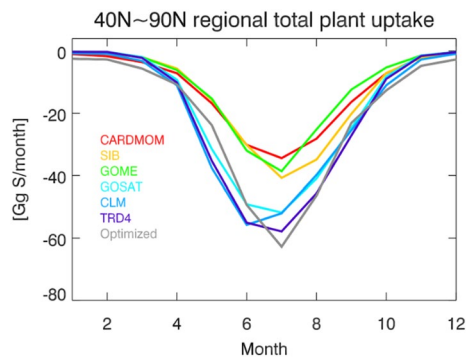


**Figure 8.** A comparison of monthly mean integrated Carbonyl Sulfide (OCS) plant uptake reveals that the models investigated fall into two distinct groups: high and low OCS uptake. The high OCS uptake models (versions 4 of the TRENDY, Community Land Model and Greenhouse Gases Observing SATellite) agree much better with our optimized run than do the low OCS uptake models (CARDAMOM, SIB, GOME). Fluxes are integrated over 40°–90° N each month.

optimized run and the CARVE measurements is dominated by inaccuracies in the FT after April and increases over time.

Looking across the model ensemble we find that on average model OCS mole fractions are biased high in BL, although several model BL estimates are within the uncertainty of CARVE BL seasonal variation. However in the FT, individual GPP-based model estimates and the ensemble mean are both biased significantly low. As a result, the ensemble mean even shows a positive vertical gradient in the spring and early summer from April – July, which is of the opposite sign to CARVE data and optimized runs (Figure 6b). Moving deeper into the growing season, we find the model “OCS uptake period,” when OCS is depleted in the BL relative to the FT, only lasts for 3–4 months from August - November. In contrast, optimized runs show the deeper magnitude and a longer period of BL depletion from April through November or later, suggesting longer and more active plant activity within Alaska than predicted by most models. The observed early spring onset is consistent with spaceborne SIF and tower-derived GPP estimates in Alaskan boreal forests (Parazoo et al., 2018).

Then we compare the observed monthly mean atmospheric OCS time series at the BRW site (tundra, left column) and CRV (boreal forest, right column) towers against our optimized run and simulations with the different GPP models in Figure 7. In these simulations, we used the same total annual flux for each simulation year. Therefore, the interannual variability in the simulations is driven solely by meteorology. Our optimized run produces reasonable seasonal amplitude and phase at both the tundra (BRW) and boreal forest (CRV) sites. The GOSAT, CLM, and TRD4 models also simulate the measured OCS seasonal amplitudes at both sites with some fidelity; however, SIB, GOME, and CARDAMOM significantly underestimate summer OCS drawdown and hence the OCS seasonal cycle amplitudes are too weak at both sites and show not enough drawdown in summer. We show later that their GPP values are systematically underestimated, while GPP estimates from the GOSAT, CLM and TRD4 models are more consistent with the OCS observational constrained GPP.

### 3.2. OCS Plant Uptake Flux Comparisons

We compare the seasonal variation of the regional scaled monthly mean OCS plant uptake values from our optimized fluxes and different GPP based OCS plant uptake fluxes that used for the different model simulations in Figure 8. Fluxes were integrated over 40–90°N in each case. Owing to the limited knowledge on plant OCS uptake at these high northern latitudes, the regional comparison between different products and optimized fluxes helps to access the plant OCS uptake in this region. GOSAT, CLM, and TRD4 have more comparable uptake magnitude with the optimized fluxes over the year than CARDAMOM, SIB and GOME, which show relative

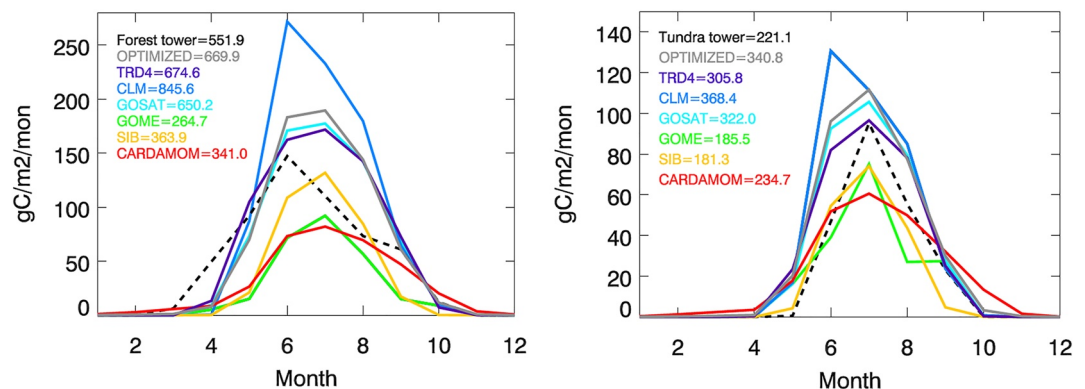


**Figure 9.** The seasonal variation of the monthly gross primary productivity (GPP) at the forest tower site and the tundra tower site from GPP models and derived observations. The legend is the annual GPP estimate in units of gC/m<sup>2</sup>/yr.

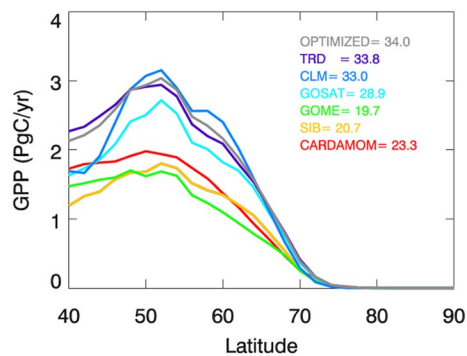


**Figure 10.** The model ensemble estimates of latitudinally dependent gross primary productivity (GPP) vary by up to 100% even at 60N, the heart of the Arctic-boreal region, and most models significantly underestimate our Carbonyl Sulfide (OCS)-optimized GPP estimate (gray line). Inset: northern high latitude integrated mean annual GPP (in units of PgC/yr) for the range 40–90N from our OCS-optimized solution and the model ensemble.

shallower uptake from spring to summer and only around half of the optimized fluxes. Peak growing season uptake occurs in July in all estimates except CLM maximized in June. GOSAT, CLM and TRD4 also show about 1 month earlier and a higher rate of uptake in the spring growing season but 5–10 Gg S/month lower uptake in July compared to the optimized phenology.

The global and regional integrated annual OCS fluxes are summarized in Table 4. The GPP models are clearly separated into two groups. The high-value group includes GOSAT, CLM, and TRD4. These GPP models have similar strong GPP and GPP-based OCS uptake fluxes. All three simulate the reasonable seasonal amplitude of OCS at both BRW and CRV sites in Figure 7. While the OCS flux and GPP from SIB, GOME and CARDAMOM are in the low-value group and they consistently simulate weak seasonal amplitudes of OCS in Figure 7 suggesting insufficient uptake and weak GPP especially from growing season to summer. The optimized flux and optimized GPP are more consistent with the three members in high-value group at the 40°N ~ 90°N region but the optimized flux and optimized GPP both agree better with the model ensemble estimate in a global scale. This suggests the GPP models bias differently in tropics and can be further studied in the future.

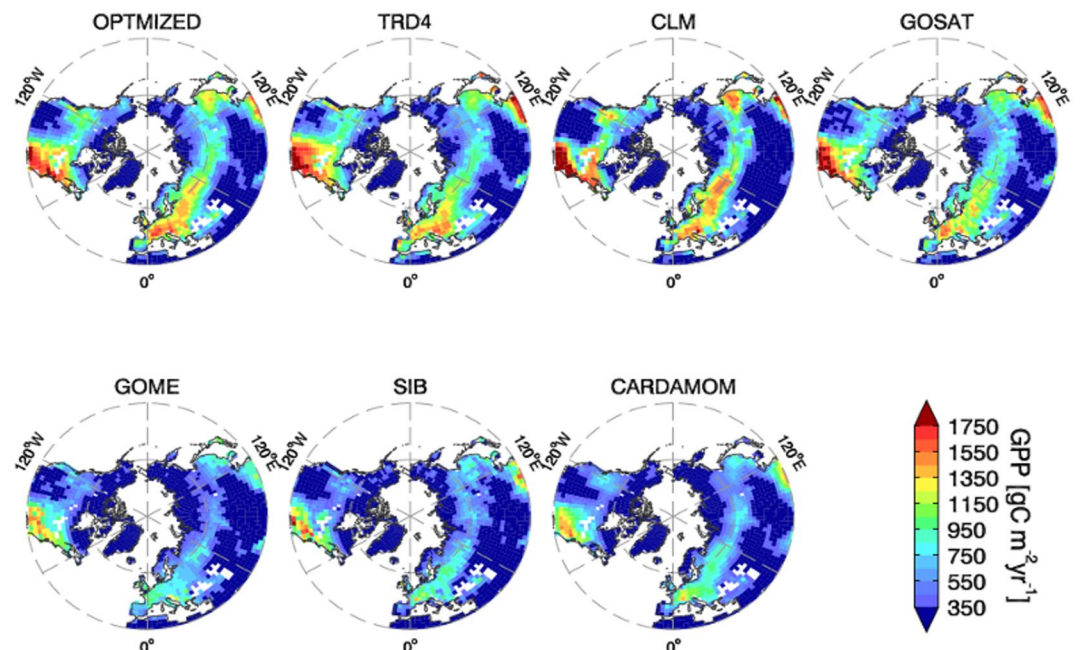


**Figure 11.** The annual gross primary productivity (GPP) maps for the comparison between the multiple models and optimal estimates of inferred GPP.

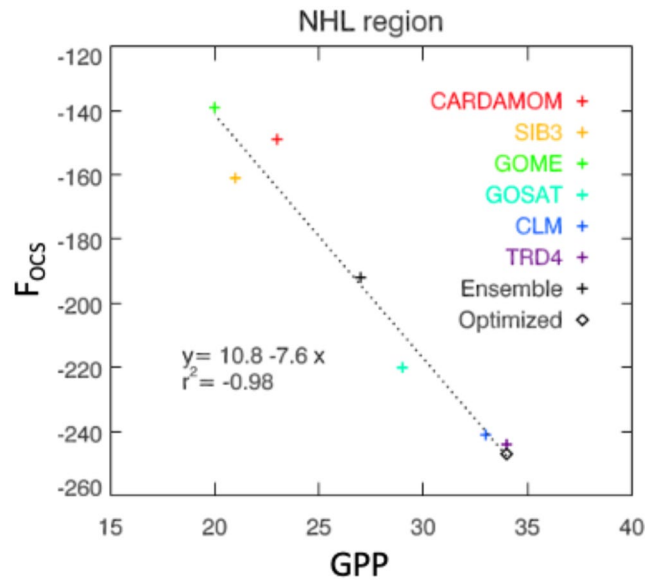


**Figure 12.** The linear anti-correlation between Carbonyl Sulfide plant uptake flux ( $F_{ocs}$ ) and gross primary productivity integrated in northern high latitude.

### 3.3. Evaluating GPP With Optimal Estimates and Flux Tower Data

To further evaluate the assumption that weak seasonality and vertical drawdown of atmospheric OCS are related to insufficient plant photosynthetic uptake, we compare OCS optimized GPP ( $GPP_{opt}$ ) to estimates of GPP from flux tower observations at two unique Alaskan tundra and boreal ecosystems (Figure 9). This plot shows a strong divergence in the summer peak and the phase of the growing and transitional period. The summer peak estimates at the forest site range widely from 80 to 260  $gC\ m^{-2}\ mon^{-1}$  while the range of the tundra site varies from 60 to 130  $gC\ m^{-2}\ mon^{-1}$ . The observed GPP suggests that the summer peak GPP value of forest sites (150  $gC/m^2/month$ ) is about 60  $gC\ m^{-2}\ mon^{-1}$  higher than the tundra site (90  $gC/m^2/month$ ), almost twice as strong as the tundra summer peak value but the GPP peak is one month earlier at forest site (June) than the tundra site (July). CLM shows an earlier (and higher) GPP peak compared to other models, which is aligned with the forest tower but too early compared to the tundra tower. Consistently, CLM, GOSAT, and TRD4 show higher GPP than SIB, GOME and CARDAMOM from April to October. The OCS-optimized GPP is most similar to GOSAT. The observed tower GPP at both sites shows a clear difference between the high GPP group including CLM, GOSAT, and TRD4 and the low GPP group including SIB, GOME and CARDAMOM.

OCS optimized GPP reproduces the different seasonal phases and amplitude of the forest and tundra towers, specifically, earlier GPP onset and higher peak amplitude at the forest tower. This is very encouraging and provides an important benchmark for modeling the seasonal phenology of Arctic ecosystems, in this case indicating better performance for GOSAT and TRD4.

However, OCS optimized GPP does not capture the extent of early GPP onset into early April at the forest tower. While CARVE collected critical profile data early in the growing season, detection of the very early start at the forest tower could be limited by (a) consistent data in April over multiple years (i.e., flights in 2012 and 2014 started in May), and (b) lack of near surface data within shallow boundary layers in the late cold season. Our first-order assumption that LRU is time-invariant might also explain wider than the observed peaks in GPP during the middle of the growing season.

A similar story emerges in a large-scale latitudinal gradient of the zonal averaged GPP from 40 to 90°N region (Figure 10), where all GPP results (model simulations and the OCS-optimized result) peak near 50°N but range widely in magnitude from 1.5 to 3  $PgC\ yr^{-1}$ . Consistent with the early analysis, the high GPP group, including GOSAT, TRD4, and CLM, varies closely with the optimal GPP but these results are higher than those in the low

GPP group, SIB, GOME, and CARDAMOM. The additional regional and annual integrated GPP from 40 to 90°N in Table 4 provide consistent evidence that weak OCS plant uptake flux is related to low GPP.

The polar-view maps of the GPP in Figure 11 show substantial spatial variation across the northern extratropics. TRD4, CLM and GOSAT, which have higher global GPP, agree much better with the OCS-optimized solution. Then the low GPP group, SIB, CARDAMOM, and GOME, have notably lower GPP values at those highlighted strong GPP regions. For example, in the Arctic Alaska region, GOSAT, TRD4, CLM and optimized GPP have comparable higher GPP values than the low GPP group (bottom row), including SIB, GOME, and CARDAMOM ( $950 \text{ gC m}^{-2} \text{ yr}^{-1}$  vs.  $500 \text{ gC m}^{-2} \text{ yr}^{-1}$ ). Other hot-spot regions including eastern North America, Northern Europe and southern boreal Siberia, show more spatial contrasts between the high GPP group and the low GPP group. The high GPP models have broader areas of hot spots with GPP close to  $1500$  or  $1700 \text{ gC m}^{-2} \text{ yr}^{-1}$  or even higher especially in eastern North America, while the low GPP models (SIB, GOME, and CARDAMOM) are only less than  $1300 \text{ gC m}^{-2} \text{ yr}^{-1}$ .

Finally, in Figure 12, we compared the annual total OCS plant uptake flux and GPP aggregated in NHL. Again, the OCS flux and GPP stay in a linear relationship among the models in NHL with  $-0.98$  anti-correlation. The model ensemble means of OCS flux and GPP are approximately 25% lower than both from optimal estimates. The individual model estimates of OCS flux and GPP from the high GPP group are well close to the optimal estimates ( $-247 \text{ Gg S yr}^{-1}$  and  $34 \text{ PgC yr}^{-1}$ ). However, the estimates of both quantities from the low GPP group members are about one third less than the optimal estimates.

#### 4. Discussion

The wide discrepancy in model-based estimates of GPP in the Arctic-Boreal Zone is well documented (e.g., Commane et al., 2017; Fisher et al., 2014; Hu et al., 2021). Previous model evaluating studies have relied on sparsely distributed towers with limited spatial footprints, or remote-sensing driven GPP products relying on imperfect satellite observations and sparse tower observations to extrapolate over space and time. This study makes use of novel atmospheric OCS observations to evaluate regional scale model estimates of pan-Arctic GPP against atmospheric data. We exploit the relationship between photochemistry and plant uptake of atmospheric OCS through stomatal conductance to make the connection between model predictions of GPP and atmospheric observations of OCS. In particular, we leverage regionally targeted airborne profiles over Alaska to calculate boundary layer enhancements or depletions of OCS and isolate local-to-regional-plant driven processes. Our analysis of spatially resolved OCS complements a recent study by Hu et al. (2021), who performed a similar analysis using spatially discrete but temporally continuous airborne OCS measurements from the US National Oceanic and Atmospheric Administration (NOAA) Global Greenhouse Gas Referencing network. Both of our main results indicate a persistent underestimation of atmospheric OCS depletion in chemical and transport models (e.g., GEOS-CHEM, PCTM). This insufficient depletion is driven by a combination of weak plant photosynthetic uptake at the surface and errors in the prescription of background OCS mole fraction.

Specifically, we find a subset of low productivity models whose projected atmospheric OCS signals, in terms of seasonal amplitude and vertical drawdown, were consistently weak compared to tower and aircraft observations. These models include the SIB process-based model, the GOME SIF constrained model, and the CARDAMOM model-data fusion product. These models show systematically low values of OCS flux and GPP across the pan-Arctic and throughout the growing season, including (a) delayed spring OCS drawdown and factor of two low summer OCS drawdown compared to CARVE optimized fluxes, (b) weak GPP compared to Alaskan tundra and boreal flux towers, (c) delayed GPP onset compared to tundra, (d) absent or negligible latitudinal GPP gradient from 40 to 60N. Moreover, GPP polar maps show similar spatial patterns to optimized GPP estimates but predicted magnitudes are consistently low across Europe, Siberia, and North America.

Given the diversity of these models, it is unlikely they share a common set of mechanisms to explain their low productivity. We do note that CARDAMOM currently does not account for cold temperature limitation in spring, which can drive low seasonal GPP amplitude in temperature limited forests including high winter GPP and low summer GPP (Stettz et al., 2021). While GOME SIF has traditionally offered a reliable measurement of GPP variability (e.g., Commane et al., 2017; Luus et al., 2017), we acknowledge previous work showing a late bias in the date of spring onset relative to tower based GPP in Alaskan boreal forests (Parazoo et al., 2018). It is also

known that the magnitude of the GOME2 SIF product analyzed here has a high bias (Kohler et al., 2015), which arises from the nature of the wide fitting window in the SIF retrieval algorithm (e.g., Parazoo et al., 2019). While our method to scale instantaneous SIF retrievals against MODIS GPP in the GOPT algorithm should buffer such spatially invariant retrieval biases (Parazoo et al., 2014), there are numerous other uncertainties related to the GOPT algorithm, along with instrument characteristics, overpass time, illumination, and view geometry differences between GOME-2 and GOSAT, that are not well accounted for. In particular, our method uses a biome-specific scaling factor to convert SIF to GPP, which lumps shrubs from Arctic and subtropical climates into the same category. While this appears to work reasonably well for afternoon snapshots from GOSAT, which sample the diurnal cycle near the midday peak across all climates and latitudes (e.g., Frankenberg et al., 2011), it is unclear how accurately this applies to morning snapshots from GOME-2, which are vulnerable to larger latitudinal differences in view geometry and illumination (e.g., Joiner et al., 2020). While we provide GOME-2 results to be comprehensive, we caution the reader that our GOME-2 GPP estimates are subject to significant uncertainty and require more detailed analysis that is beyond the scope of this study.

Finally, it is still unclear which factors contribute to low productivity in SIB, though it is noted that a previous investigation of SIB at a subalpine evergreen forest in Colorado also found a low bias in GPP in simulations with Leaf Area Index prescribed using satellite observations from MODIS, rather than using observations by the tower (Parazoo et al., 2020).

We find another subset of high productivity models, including GOSAT, CLM, and TRD4, which simulate reasonable or even stronger seasonal variation in OCS concentration but are still prone to weak vertical drawdown due to low background mole fractions. Both the OCS-constrained regional GPP and flux tower GPP suggest that highly productive GPP, such as from GOSAT, CLM, and TRD4 provide GPP strong enough to simulate the OCS vertical drawdown and seasonal variation in Alaska. The high performance of GOSAT is consistent with previous findings, and it is encouraging to see good agreement with tower data and optimized fluxes at high latitudes. CLM shows reasonable agreement with optimized OCS seasonality, and the tendency for early growing spring onset has been previously documented and attributed in part to the formulation of leaf budburst, which is improved when accounting for cold temperature effects (Shi et al., 2020). The close agreement between TRD4 and optimized OCS flux and GPP supports previous findings that model ensemble averages tend to provide improved estimates of GPP compared to individual models, especially at high latitudes (e.g., Fisher et al., 2014).

We note several important caveats in this study which are likely to affect the use of OCS as a proxy for model GPP. In particular, this analysis relies on the use of global transport modeling to simulate the distribution of OCS in the atmosphere for comparison to tower and aircraft data. We first note that global atmospheric simulations are already challenging in trying to account for the multiple horizontal and vertical mixing processes which are highly unresolved at the coarse  $2.5 \times 2^\circ$  resolution used here. The use of reanalysis data to drive the model helps, but vertical mixing remains a challenge, especially in the Arctic given the complex topography and surface energy exchanges.

The majority change of the optimized OCS flux to the prior flux suggests higher GPP model is preferred to generate reasonable vertical profiles in the simulations. Consistently, Hu et al., 2021 suggested higher OCS-optimized GPP than SIB4 over the North American Arctic and Boreal region (5%–15% increase in April–September and 30%–50% increase in October–March). Meanwhile, the stronger optimized OCS uptake flux may result from other underestimated processes besides GPP such as soil uptake, and nighttime plant uptake while incompletely closed stomata (Hu et al., 2021) and dry deposition. OCS diffuses through stomata into leaves where it is consumed by Carbonic Anhydrase. Reduced OCS in leaves creates a positive OCS gradient from the canopy air to the leaves during the night. The uptake will be small but not zero during the night because stomatal conductance is not completely closed. There will be a small but non-negligible uptake inside the leaf throughout the night. Hu et al., 2021 showed that their OCS inversion suggests that nighttime uptake should be higher than the SIB4 nighttime uptake.

The dry deposition is known to cause ozone and methane loss at the surface. A similar non-photosynthetic uptake of OCS might account for part of the model-data discrepancy. Currently, we are not able to differentiate the updates of the flux from these processes and from GPP. However, the amount of these processes is much smaller than that from the GPP.

There is also a mismatch in scale in comparing coarse grid boxes to in situ atmospheric mole fractions. We also find that the background influences on OCS are not well constrained. Even though global modeling accounts for global oceanic and terrestrial influences, the magnitude of these sources, in particular ocean dimethyl-sulfide (DMS) emissions, are not well known. Finally, in building the linear model to convert predicted GPP to OCS, we assume that the equations for photochemistry and CO<sub>2</sub> diffusion into leaves are both well known, linearly related, and scale across common plant functional types.

Nevertheless, we provide a novel and potentially valuable framework for evaluating model photosynthesis in the Arctic. Our approach can easily be applied to other regions in North America and Europe where more airborne OCS observations are made. It would be particularly useful to determine whether such an approach can be used with long term records from the NOAA airborne network to track changes in regional photosynthesis over inter-annual to decadal time scales.

## 5. Conclusions

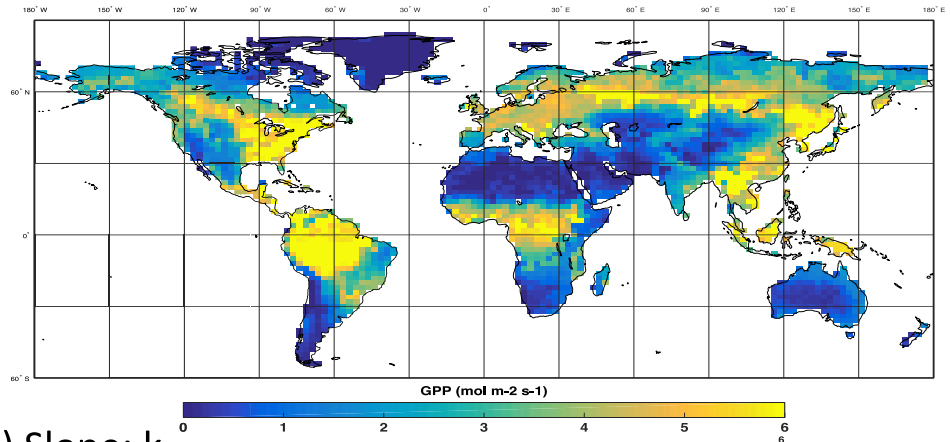
We used atmospheric OCS mole fraction observations from ground sites (BRW and CRV) and aircraft campaigns (CARVE) to evaluate the model simulations with different plant uptake fluxes derived from a diverse set of GPP products. We found a subset of low terrestrial productivity models including SIB, GOME, CARDAMOM whose projected atmospheric OCS uptake signals, in terms of seasonal amplitude and vertical drawdown, were consistently weak compared to observations. Another subset of high productivity models including GOSAT, CLM, and TRD4 simulate more reasonable or even stronger seasonal variation but are still prone to weak vertical drawdown due to low background mole fractions. Both the OCS constrained regional GPP and flux tower GPP suggest that highly productive models, GOSAT, CLM, and TRD4 provide GPP strong enough to simulate the OCS vertical drawdown and seasonal variation in Alaska. SIB, GOME and CARDAMOM GPP products at the northern extra-tropic are overall too weak, in particular in Northern midlatitude Eurasia, Siberia, Eastern North America, and Arctic Alaska. Quantitatively, we suggest 33 PgC yr<sup>-1</sup> GPP for the region of 40°N ~90°N and 247 Gg S yr<sup>-1</sup> plant uptake for OCS in the region.

Our study indicates from the OCS constraint that regional GPP at high latitude is likely encompassed by the multi-model range of GPP. These modeled GPP are still incapable of starting the growing season at the correct timing over both forest and tundra sites. A more comprehensive inversion method with OCS observations in a finer spatial-temporal resolution is expected to help to further improve the performance in the phenology in the current GPP. A more extensive observational system of OCS with multiple platforms including additional ground-based measurements, airborne and satellite remote sensing data is the next step to advance the study to improve current GPP through OCS for carbon uptake in the mid-to high-latitude terrestrial ecosystem.

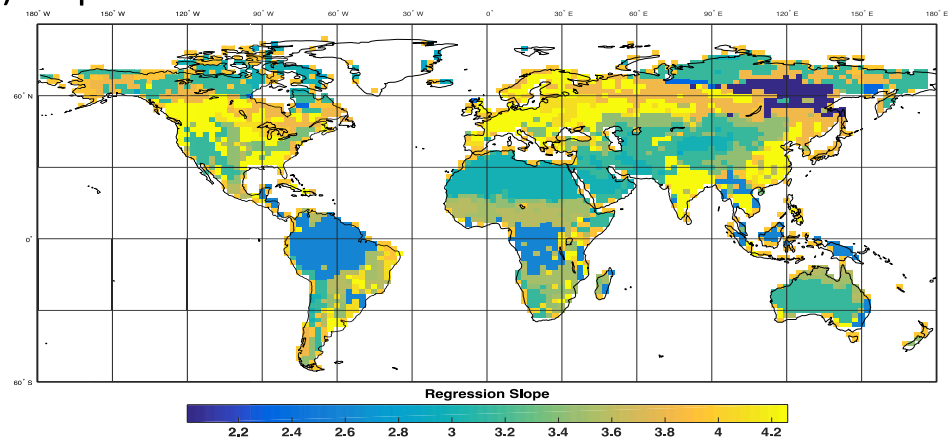
In this study, we try to justify the effectiveness of using OCS to estimate GPP. We acknowledge that Leaf Area Index (LAI) and physiology are crucial to GPP estimation in terrestrial biosphere models (TBMs). For example, LAI of each canopy layer is used to integrate foliage photosynthesis to canopy photosynthesis in CLM, and this model representation suggests that plant physiology (e.g., carbon allocation) and LAI are closely related to the GPP simulations (Lawrence et al., 2019). Daily LAI is also used to estimate sub-daily photosynthetic assimilation in the Simple Biosphere Mode (SIB; Lokupitiya et al., 2009). These model structures can be understood as that LAI is a proxy of stomatal density, which regulates the intensity of leaf-level carbon flux exchanges, including OCS. Site-level LAI measurements at varied canopy layers can benefit the upscaling of leaf-level GPP and OCS fluxes to the canopy-level and ecosystem level, and are essential to the top-down and bottom-up comparisons and understanding of terrestrial carbon fluxes. LAI measurements at different scales (e.g., in situ and satellite) are also key to interpreting the seasonal dynamics of GPP and OCS fluxes at varied spatiotemporal resolutions. This research justifies the substantial role of OCS in estimating GPP, which could be controlled by environmental factors (e.g., temperature, water, and sun light) decided stomatal dynamics and the plant physiology of varied terrestrial ecosystems (e.g., the onset of the growing season), and paves a way for estimating GPP at varied scales and for further understanding terrestrial carbon dynamics with this new framework.

Appendix A

(a) SIF-GPP



(b) Slope: k



(c) SIF-OCS flux

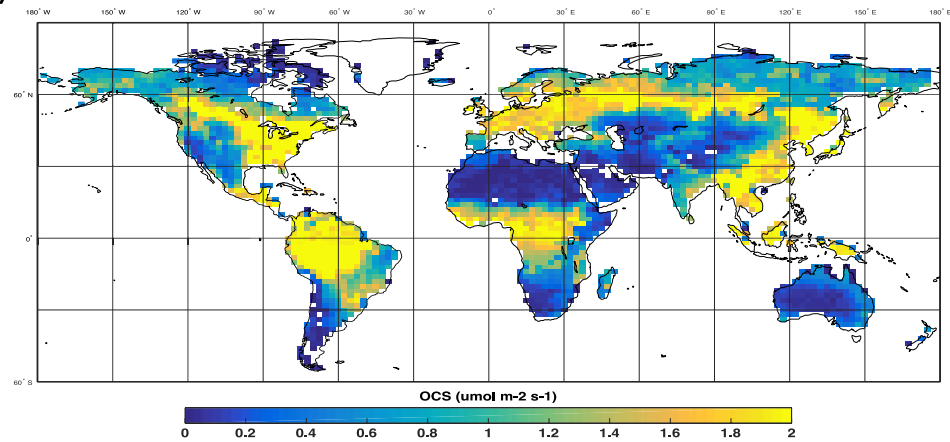


**Figure A1.** (a) Solar induced chlorophyll fluorescence (SIF) optimized gross primary productivity (GPP) (SIF-GPP); (b) Regression slope of SIF-GPP and SIF-Carbonyl Sulfide (OCS) plant uptake flux; (c) Inferred OCS flux from SIF GPP using linear regression parameters and Equation 1.

## Data Availability Statement

CARVE observations for all the campaigns from 2012 to 2016 are archived at ORNL DAAC ([https://daac.ornl.gov/cgi-bin/dataset\\_lister.pl?p=35](https://daac.ornl.gov/cgi-bin/dataset_lister.pl?p=35)). The ground-based OCS measurements at BRW and CRV are available at NOAA/GML website (<https://gml.noaa.gov/dv/data/>). The GPP data from all models, OCS fluxes and GEOS-CHEM model simulations are available upon request, and will be archived during the reviewing process.

## Acknowledgments

This research was carried out at the Jet Propulsion Laboratory, California Institute of Technology, under a contract with the National Aeronautics and Space Administration (NASA). This study was funded by CARVE project. LK was also supported by the National Aeronautics and Space Administration (NASA), United States (ECOSTRESS Science and Applications Team: Grant No. 80NSSC20K0215). SAM acknowledges the technical contributions and support of C. Siso, B. Miller, I. Vimont, A. Andrews, J. Higgs, S. Wolter, D. Neff, and other NOAA and CIRES colleagues that enabled the NOAA/GML sampling and sample analyses used in this study. MS carried this work with the support of the NASA Grant 80NSSC20K0215, and PNNL is operated by Battelle Memorial Institute for the U.S. DOE under contract DE-AC05-76RLO1830. The authors want to acknowledge the 2017 Keck Institute for Space Studies workshop “Next-Generation Approach for Detecting Climate-Carbon Feedbacks: Space-Based Integration of Carbonyl Sulfide (OCS), CO<sub>2</sub>, and Solar Induced Fluorescence (SIF)” and the helpful discussion during the workshop.

## References

- Anav, A., Friedlingstein, P., Beer, C., Ciais, P., Harper, A., Jones, C., et al. (2015). Spatiotemporal patterns of terrestrial gross primary production: A review. *Reviews of Geophysics*, 53(3), 785–818. <https://doi.org/10.1002/2015RG000483>
- Baier, B. C., Sweeney, C., Choi, Y., Davis, K. J., Di Gangi, J. P., Feng, S., et al. (2020). Multispecies assessment of factors influencing regional CO<sub>2</sub> and CH<sub>4</sub> enhancements during the winter 2017 ACT-America campaign. *Journal of Geophysical Research: Atmospheres*, 125(2), e2019JD031339. <https://doi.org/10.1029/2019JD031339>
- Baker, I. T., Denning, A. S., Hanan, N., Prihodko, L., Vidale, P.-L., Davis, K., & Bakwin, P. (2003). Simulated and observed fluxes of sensible and latent heat and CO<sub>2</sub> at the WLEF-TV Tower using SiB2.5. *Global Change Biology*, 9, 1262–1277. <https://doi.org/10.1046/j.1365-2486.2003.00671.x>
- Baker, I. T., Prihodko, L., Denning, A. S., Goulden, M., Miller, S., & Rocha, H. R. (2008). Seasonal drought stress in the Amazon: Reconciling models and observations. *Journal of Geophysical Research*, 113(G1), 1–10. <https://doi.org/10.1029/2007JG000644>
- Baldocchi, D., Chu, H., & Reichstein, M. (2018). Inter-annual variability of net and gross ecosystem carbon fluxes: A review. *Agricultural and Forest Meteorology*, 249, 520–533. <https://doi.org/10.1016/j.agrformet.2017.05.015>
- Barnes, E. A., Parazoo, N., Orbe, C., & Denning, A. S. (2016). Isentropic transport and the seasonal cycle amplitude of CO<sub>2</sub>. *Journal of Geophysical Research: Atmospheres*, 121(13), 8106–8124. <https://doi.org/10.1002/2016JD025109>
- Berry, J., Wolf, A., Campbell, J. E., Baker, I., Blake, N., Blake, D., et al. (2013). A coupled model of the global cycles of carbonyl sulfide and CO<sub>2</sub>: A possible new window on the carbon cycle. *Journal of Geophysical Research: Biogeosciences*, 118(2), 842–852. <https://doi.org/10.1002/jgrg.20068>
- Bloom, A. A., Exbrayat, J.-F., van der Velde, I. R., Feng, L., & Williams, M. (2016). The decadal state of the terrestrial carbon cycle: Global retrievals of terrestrial carbon allocation, pools, and residence times. *Proceedings of the National Academy of Sciences of the United States of America*, 113(5), 1285–1290. <https://doi.org/10.1073/pnas.1515160113>
- Byrne, B., Wunch, D., Jones, D. B. A., Strong, K., Deng, F., Baker, I., et al. (2018). Evaluating GPP and respiration estimates over northern midlatitude ecosystems using solar induced fluorescence and atmospheric CO<sub>2</sub> measurements. *Journal of Geophysical Research: Biogeosciences*, 123(9), 2976–2997. <https://doi.org/10.1029/2018JG004472>
- Campbell, J. E., Carmichael, G. R., Chai, T., Mena-Carrasco, M., Tang, Y., Blake, D. R., et al. (2008). Photosynthetic control of atmospheric carbonyl sulfide during the growing season. *Science*, 322(5904), 1085–1088. <https://doi.org/10.1126/science.1164015>
- Campbell, J. E., Laine, M., Stinecipher, J., Kuai, L., Wang, C., Zhu, K., et al. (in press). Cameron-Smith: Seasonal amplitude reversal in atmospheric carbonyl sulfide.
- Campbell, J. E., Whelan, M. E., Seibt, U., Smith, S. J., Berry, J. A., & Hilton, T. W. (2015). Atmospheric carbonyl sulfide sources from anthropogenic activity: Implications for carbon cycle constraints. *Geophysical Research Letters*, 42(8), 3004–3010. <https://doi.org/10.1002/2015GL063445>
- Commans, R., Lindaas, J., Benmergui, J., Luus, K. A., Chang, R. Y.-W., Daube, B. C., et al. (2017). Carbon dioxide sources from Alaska driven by increasing early winter respiration from Arctic tundra. *Proceedings of the National Academy of Sciences of the United States of America*, 114(21), 5361–5366. <https://doi.org/10.1073/pnas.1618567114>
- Commans, R., Meredith, L. K., Baker, I. T., Berry, J. A., Munger, J. W., Montzka, S. A., et al. (2015). Seasonal fluxes of carbonyl sulfide in a midlatitude forest. *Proceedings of the National Academy of Sciences of the United States of America*, 112(46), 14162–14167. <https://doi.org/10.1073/pnas.1504131112>
- Euskirchen, E. S., Bret-Harte, M. S., Shaver, G. R., Edgar, C. W., & Romanovsky, V. E. (2017). Long-term release of carbon dioxide from arctic tundra ecosystems in Alaska. *EOSSystems*, 20(5), 960–974. <https://doi.org/10.1007/s10021-016-0085-9>
- Euskirchen, E. S., Carman, T. B., & McGuire, A. D. (2014). Changes in the structure and function of northern Alaskan ecosystems when considering variable leaf-out times across groupings of species in a dynamic vegetation model. *Global Change Biology*, 20(3), 963–978. <https://doi.org/10.1111/gcb.12392>
- Fisher, J. B., Hayes, D. J., Schwalm, C. R., Huntzinger, D. N., Stofferahn, E., Schaefer, K., et al. (2018). Missing pieces to modeling the Arctic-Boreal puzzle. *Environmental Research Letters*, 13(2), 020202. <https://doi.org/10.1088/1748-9326/aa9d9a>
- Fisher, J. B., Sikka, M., Oechel, W. C., DeborahHuntzinger, N., Melton, J. R., Koven, C. D., et al. (2014). Carbon cycle uncertainty in the Alaskan Arctic. *Biogeosciences*, 11(15), 4271–4288. <https://doi.org/10.5194/bg-11-4271-2014>
- Forkel, M., Carvalhais, N., Rödenbeck, C., Keeling, R., Heimann, M., Thonicke, K., et al. (2016). Enhanced seasonal CO<sub>2</sub> exchange caused by amplified plant productivity in northern ecosystems. *Science*, 351(6274), 696–699. <https://doi.org/10.1126/science.aac4971>
- Frankenberg, C., Butz, A., & Toon, G. C. (2011). Disentangling chlorophyll fluorescence from atmospheric scattering effects in O<sub>2</sub> A-band spectra of reflected sun-light. *Geophysical Research Letters*, 38(3). <https://doi.org/10.1029/2010gl045896>
- Glatthor, N., Hopfner, M., Baker, I. T., Berry, J., Campbell, J. E., Kawa, S. R., et al. (2015). Tropical sources and sinks of carbonyl sulfide observed from space. *Geophysical Research Letters*, 42(22), 10082–10090. <https://doi.org/10.1002/2015GL066293>
- Glatthor, N., Höpfner, M., Leyser, A., Stiller, G. P., von Clarmann, T., Grabowski, U., et al. (2017). Global carbonyl sulfide (OCS) measured by MIPAS/Envisat during 2002–2012. *Atmospheric Chemistry and Physics*, 17(4), 2631–2652. <https://doi.org/10.5194/acp-17-2631-2017>
- Graven, H. D., Keeling, R. F., Piper, S. C., Patra, P. K., Stephens, B. B., Wofsy, S. C., et al. (2013). Enhanced seasonal exchange of CO<sub>2</sub> by Northern ecosystems since 1960. *Science*, 341(6150), 1085–1089. <https://doi.org/10.1126/science.1239207>
- Hilton, T. W., Whelan, M. E., Zumkehr, A., Kulkarni, S., Berry, J. A., Baker, I. T., et al. (2017). Peak growing season gross uptake of carbon in North America is largest in the Midwest USA. *Nature Climate Change*, 7(6), 450–454. <https://doi.org/10.1038/nclimate3272>
- Hinzman, L. D., Deal, C. J., McGuire, A. D., Mermild, S. H., Polyakov, I. V., Walsh, J. E., et al. (2013). Trajectory of the Arctic as an integrated system. *Ecological Applications*, 23(8), 1837–1868. <https://doi.org/10.1890/11-1498.1>
- Hu, L., Montzka, S. A., Kaushik, A., Andrews, A. E., Sweeney, C., Miller, J., et al. (2021). COS-derived GPP relationships with temperature and light help explain high-latitude atmospheric CO<sub>2</sub> seasonal cycle amplification. *Proceedings of the National Academy of Sciences of the United States of America*, 118(33), e2103423118. <https://doi.org/10.1073/pnas.2103423118>

- Jeong, S. J., Bloom, A. A., Schimel, D., Sweeney, C., Parazoo, N. C., Medvigy, D., et al. (2018). Accelerating rates of arctic carbon cycling revealed by long-term atmospheric CO<sub>2</sub> measurements. *Science Advances*, 4(7), 1–7. <https://doi.org/10.1126/sciadv.aao1167>
- Joiner, J., Yoshida, Y., Köehler, P., Campbell, P., Frankenberg, C., van der Tol, C., et al. (2020). Systematic orbital geometry-dependent variations in satellite solar-induced fluorescence (SIF) retrievals. *Remote Sensing*, 12(15), 2346. <https://doi.org/10.3390/rs12152346>
- Karion, A., Sweeney, C., Miller, J. B., Andrews, A. E., Commane, R., Dinardo, S., et al. (2016). Investigating Alaskan methane and carbon dioxide fluxes using measurements from the CARVE tower. *Atmospheric Chemistry and Physics*, 16(8), 5383–5398. <https://doi.org/10.5194/acp-16-5383-2016>
- Keenan, T. F., & Riley, W. J. (2018). Greening of the land surface in the world's cold regions consistent with recent warming. *Nature Climate Change*, 8(9), 825–828. <https://doi.org/10.1038/s41558-018-0258-y>
- Kettle, A. J., Kuhn, U., von Hobe, M. V., Kesselmeier, J., & Andreae, M. O. (2002). Global budget of atmospheric carbonyl sulfide: Temporal and spatial variations of the dominant sources and sinks. *Journal of Geophysical Research*, 107(D22), ACH-25. <https://doi.org/10.1029/2002jd002187>
- Köhler, P., Guanter, L., & Joiner, J. (2015). A linear method for the retrieval of sun-induced chlorophyll fluorescence from GOME-2 and SCIAMACHY data. *Atmospheric Measurement Techniques*, 8(6), 2589–2608. <https://doi.org/10.5194/amt-8-2589-2015>
- Kooijmans, L. M. J., Cho, A., Ma, J., Kaushik, A., Haynes, K. D., Baker, I., et al. (2021). Evaluation of carbonyl sulfide biosphere exchange in the Simple Biosphere Model (SiB4). *Biogeosciences*, 18(24), 6547–6565. <https://doi.org/10.5194/bg-18-6547-2021>
- Kuai, L., Worden, J., Kulawik, S. S., Montzka, S. A., & Liu, J. (2014). Characterization of Aura TES carbonyl sulfide retrievals over ocean. *Atmospheric Measurement Techniques*, 7(1), 163–172. <https://doi.org/10.5194/amt-7-163-2014>
- Kuai, L., Worden, J. R., Campbell, J. E., Kulawik, S. S., Li, K.-F., Lee, M., et al. (2015). Estimate of carbonyl sulfide tropical oceanic surface fluxes using Aura Tropospheric Emission Spectrometer observations. *Journal of Geophysical Research: Atmospheres*, 120(20), 11012–11023. <https://doi.org/10.1002/2015JD023493>
- Lasslop, G., Reichstein, M., Papale, D., Richardson, A., Arneeth, A., Barr, A., et al. (2010). Separation of net ecosystem exchange into assimilation and respiration using a light response curve approach: Critical issues and global evaluation. *Global Change Biology*, 16(1), 187–208. <https://doi.org/10.1111/j.1365-2486.2009.02041.x>
- Lawrence, D. M., Fisher, R. A., Koven, C. D., Oleson, K. W., Swenson, S. C., & Bonan, G. (2019). The Community Land Model version 5: Description of new features, benchmarking, and impact of forcing uncertainty. *Journal of Advances in Modeling Earth Systems*, 11(12), 4245–4287. <https://doi.org/10.1029/2018ms001583>
- Lennartz, S. T., Gauss, M., von Hobe, M., & Marandino, C. A. (2021). Monthly resolved modelled oceanic emissions of carbonyl sulphide and carbon disulphide for the period 2000–2019. *Earth System Science Data*, 13(5), 2095–2110. <https://doi.org/10.5194/essd-13-2095-2021>
- Liu, J., Wennberg, P. O., Parazoo, N. C., Yin, Y., & Frankenberg, C. (2020). Observational constraints on the response of high-latitude northern forests to warming. *AGU Advances*, 1(4), e2020AV000228. <https://doi.org/10.1029/2020av000228>
- Liu, Z., Kimball, J. S., Parazoo, N. C., Ballantyne, A. P., Wang, W. J., Madani, N., et al. (2020). Increased high-latitude photosynthetic carbon gain offset by respiration carbon loss during an anomalous warm winter to spring transition. *Global Change Biology*, 26(2), 682–696. <https://doi.org/10.1111/gcb.14863>
- Lokupitiya, E., Denning, S., Paustian, K., Baker, I., Schaefer, K., Verma, S., et al. (2009). Incorporation of crop phenology in Simple Biosphere Model (SiBcrop) to improve land-atmosphere carbon exchanges from croplands. *Biogeosciences*, 6(6), 969–986.
- Lorant, M. M., & Goetz, S. J. (2012). Shrub expansion and climate feedbacks in Arctic tundra. *Environmental Research Letters*, 7(1), 011005. <https://doi.org/10.1088/1748-9326/7/1/011005>
- Luus, K. A., Commane, R., Parazoo, N. C., Benmergui, J., Euskirchen, E. S., Frankenberg, C., et al. (2017). Tundra photosynthesis captured by satellite-observed solar-induced chlorophyll fluorescence. *Geophysical Research Letters*, 44(3), 1564–1573. <https://doi.org/10.1002/2016gl070842>
- Maseyk, K., Berry, J. A., Billesbach, D., Campbell, J. E., Torn, M. S., Zahniser, M., & Seibt, U. (2014). Sources and sinks of carbonyl sulfide in an agricultural field in the Southern Great Plains. *Proceedings of the National Academy of Sciences*, 111(25), 9064–9069. <https://doi.org/10.1073/pnas.1319132111>
- McGuire, A. D., Lawrence, D. M., Koven, C., Clein, J. S., Burke, E., Chen, G., et al. (2018). Dependence of the evolution of carbon dynamics in the northern permafrost region on the trajectory of climate change. *Proceedings of the National Academy of Sciences of the United States of America*, 115(15), 3882–3887. <https://doi.org/10.1073/pnas.1719903115>
- Miller, C. E., & Dinardo, S. J., & CARVE Science, Team. (2012). CARVE: The carbon in arctic Reservoirs vulnerability experiment. *IEEE Aerospace Conf.* <https://doi.org/10.1109/AERO.2012.6187026>
- Miller, J. B., Sweeney, C., Karion, A., & Miller, C. E. (2016). CARVE: L2 atmospheric gas mole fractions, tower-based flasks, Alaska, 2012–2015. ORNL DAAC. <https://doi.org/10.3334/ORNLDAAC/1405>
- Montzka, S. A., Calvert, P., Hall, B. D., Elkins, J. W., Conway, T. J., Tans, P. P., & Sweeney, C. (2007). On the global distribution, seasonality, and budget of atmospheric carbonyl sulfide (OCS) and some similarities to CO<sub>2</sub>. *Journal of Geophysical Research*, 112(D9), D09302. <https://doi.org/10.1029/2006JD007665>
- Myers-Smith, I. H., Forbes, B. C., Wilmking, M., Hallinger, M., Lantz, T., Blok, D., et al. (2011). Shrub expansion in tundra ecosystems: Dynamics, impacts and research priorities. *Environmental Research Letters*, 6(4), 045509. <https://doi.org/10.1088/1748-9326/6/4/045509>
- Myers-Smith, I. H., Myers-Smith, I. H., Kerby, J. T., Phoenix, G. K., Bjerke, J. W., Epstein, H. E., et al. (2020). Complexity revealed in the greening of the Arctic. *Nature Climate Change*, 10(2), 106–117. <https://doi.org/10.1038/s41558-019-0688-1>
- Natali, S. M., Watts, J. D., Rogers, B. M., Potter, S., Ludwig, S. M., Selbmann, A. K., et al. (2019). Large loss of CO<sub>2</sub> in winter observed across the northern permafrost region. *Nature Climate Change*, 9(11), 852–857. <https://doi.org/10.1038/s41558-019-0592-8>
- Norton, A. J., Rayner, P. J., Koffi, E. N., Scholze, M., Silver, J. D., & Wang, Y.-P. (2019). Estimating global gross primary productivity using chlorophyll fluorescence and a data assimilation system with the BETHY-SCOPE model. *Biogeosciences*, 16(15), 3069–3093. <https://doi.org/10.5194/bg-16-3069-2019>
- Oleson, K. W., Lawrence, D. M., Bonan, G. B., Drewniak, B., Huang, M., Charles, D., et al. (2013). CLM 4.5 NCAR technical note. <https://doi.org/10.1007/s11538-011-9690-0>
- Papale, D., Reichstein, M., Aubinet, M., Canfora, E., Bernhofer, C., Kutsch, W., et al. (2006). Towards a standardized processing of net ecosystem exchange measured with eddy covariance technique: Algorithms and uncertainty estimation. *Biogeosciences*, 3(4), 571–583. <https://doi.org/10.5194/bg-3-571-2006>
- Parazoo, N. C., Arneeth, A., Pugh, T. A. M., Smith, B., Steiner, N., Luus, K., et al. (2018). Spring photosynthetic onset and net CO<sub>2</sub> uptake in Alaska triggered by landscape thawing. *Global Change Biology*, 24(8), 3416–3435. <https://doi.org/10.1111/gcb.14283>

- Parazoo, N. C., Bowman, K., Baier, B., Liu, J., Lee, M., Kuai, L., et al. (2021). Covariation of airborne biogenic tracers (CO<sub>2</sub>, OCS, and CO) supports stronger than expected growing season photosynthetic uptake in the southeastern US. *Global Biogeochemical Cycle*. *ESSOAr*. <https://doi.org/10.1002/essoar.10505574.1>
- Parazoo, N. C., Bowman, K., Fisher, J. B., Frankenberg, C., Jones, D. B. A., Cescatti, A., et al. (2014). Terrestrial gross primary production inferred from satellite fluorescence and vegetation models. *Global Change Biology*, *20*(10), 3103–3121. <https://doi.org/10.1111/gcb.12652>
- Parazoo, N. C., Commane, R., Wofsy, S. C., Koven, C. D., Sweeney, C., Lawrence, D. M., et al. (2016). Detecting regional patterns of changing CO<sub>2</sub> flux in Alaska. *Proceedings of the National Academy of Sciences of the United States of America*, *113*(28), 7733–7738. <https://doi.org/10.1073/pnas.1601085113>
- Parazoo, N. C., Frankenberg, C., Köhler, P., Joiner, J., Yoshida, Y., Magney, T., et al. (2019). Towards a harmonized long-term spaceborne record of far-red solar-induced fluorescence. *Journal of Geophysical Research: Biogeosciences*, *124*(8), 2518–2539. <https://doi.org/10.1029/2019jg005289>
- Parazoo, N. C., Magney, T., Norton, A., Raczka, B., Bacour, C., Maignan, F., et al. (2020). Wide discrepancies in the magnitude and direction of modeled solar-induced chlorophyll fluorescence in response to light conditions. *Biogeosciences*, *17*(13), 3733–3755. <https://doi.org/10.5194/bg-17-3733-2020>
- Reichstein, M., Falge, E., Baldocchi, D., Papale, D., Aubinet, M., Berbigier, P., et al. (2005). On the separation of net ecosystem exchange into assimilation and ecosystem respiration: Review and improved algorithm. *Global Change Biology*, *11*(9), 1424–1439. <https://doi.org/10.1111/1j.1365-2486.2005.001002>
- Rogers, A., Serbin, S. P., & Way, D. A. (2021). Reducing model uncertainty of climate change impacts on high latitude carbon assimilation. *Global Change Biology*, *28*(4), 1222–1247. (BNL-222318-2021-JAAM). <https://doi.org/10.1111/gcb.15958>
- Sarmiento, J. L., & Wofsy, S. C. (1999). *A US carbon cycle science plan. A report of the carbon and climate working group* (Vol. 69). US Global Change Research Program.
- Schimel, D., Pavlick, R., Fisher, J. B., Asner, G. P., Saatchi, S., Townsend, P., et al. (2015). Observing terrestrial ecosystems and the carbon cycle from space. *Global Change Biology*, *21*(5), 1762–1776. <https://doi.org/10.1111/gcb.12822>
- Schimel, D., & Schneider, F. D. (2019). Flux towers in the sky: Global ecology from space. *New Phytologist*, *224*(2), 570–584. <https://doi.org/10.1111/nph.15934>
- Seibt, U., Kesselmeier, J., Sandoval-Soto, L., Kuhn, U., & Berry, J. A. (2010). A kinetic analysis of leaf uptake of OCS and its relation to transpiration, photosynthesis and carbon isotope fractionation. *Biogeosciences*, *7*(1), 333–341. <https://doi.org/10.5194/bg-7-333-2010>
- Shi, M., Parazoo, N. C., Jeong, S., Birch, L., Lawrence, P., Euskirchen, E. S., & Miller, C. E. (2020). Exposure to cold temperature affects the spring phenology of Alaskan deciduous vegetation types Exposure to cold temperature affects the spring phenology of Alaskan deciduous vegetation types. *Environmental Research Letters*, *15*(2), 025006. <https://doi.org/10.1088/1748-9326/ab6502>
- Sitch, S., Friedlingstein, P., Gruber, N., Jones, S. D., Murray-Tortarolo, G., Ahlström, A., et al. (2015). Recent trends and drivers of regional sources and sinks of carbon dioxide. *Biogeosciences*, *12*(3), 653–679. <https://doi.org/10.5194/bg-12-653-2015>
- Stettz, S. G., Parazoo, N. C., Bloom, A. A., Blanken, P. D., Bowling, D. R., Burns, S. P., et al. (2021). Resolving temperature limitation on spring productivity in an evergreen conifer forest using a model-data fusion framework. *Biogeosciences Discussions*, *19*(2), 541–558. <https://doi.org/10.5194/bg-2021-152>
- Stinecipher, J. R., Cameron-Smith, P., Blake, N., Kuai, L., Lejeune, B., Mahieu, E., et al. (2019). Campbell: Biomass burning unlikely to account for missing source of carbonyl sulfide. *Geophysical Research Letters*, *46*(24), 14912–14920. <https://doi.org/10.1029/2019GL085567>
- Stockli, R., & Vidale, P. L. (2005). Modeling diurnal to seasonal water and heat exchanges at European Fluxnet sites. *Theoretical and Applied Climatology*, *80*(2–4), 2–4. <https://doi.org/10.1007/s00704-004-0102-3>
- Sun, Y., Frankenberg, C., Wood, J. D., Schimel, D. S., Jung, M., Guanter, L., et al. (2017). OCO-2 advances photosynthesis observation from space via solar-induced chlorophyll fluorescence. *Science*, *358*(6360). <https://doi.org/10.1126/science.aam5747>
- Suntharalingam, P., Kettle, A. J., Montzka, S. M., & Jacob, D. J. (2008). Global 3-D model analysis of the seasonal cycle of atmospheric carbonyl sulfide: Implications for terrestrial vegetation uptake. *Geophysical Research Letters*, *35*(19), L19801. <https://doi.org/10.1029/2008GL034332>
- Sweeney, C., Chatterjee, A., Wolter, S., McKain, K., Bogue, R., Newberger, T., et al. (2020). Atmospheric carbon cycle dynamics over the ABoVEDomain: An integrated analysis using aircraft observations (Arctic-CAP) and model simulations (GEOS). *Atmospheric Chemistry and Physics Discussions*, 1–30. <https://doi.org/10.5194/acp-2020-609>
- Sweeney, C., Karion, A., Wolter, S., Newberger, T., Guenther, D., Higgs, J. A., et al. (2015). Seasonal climatology of CO<sub>2</sub> across North America from aircraft measurements in the NOAA/ESRL global greenhouse gas reference network. *Journal of Geophysical Research: Atmospheres*, *120*(10), 5155–5190. <https://doi.org/10.1002/2014JD022591>
- Sweeney, C., Miller, J. B., Karion, A., Dinardo, S. J., & Miller, C. E. (2016). *CARVE: L2 atmospheric gas mole fractions, airborne flasks, Alaska, 2012-2015*. ORNL DAAC. <https://doi.org/10.3334/ORNLDAAC/1404>
- Ueyama, M., Iwata, H., Harazono, Y., Euskirchen, E. S., Oechel, W. C., & Zona, D. (2013). Growing season and spatial variations of carbon fluxes of Arctic and boreal ecosystems in Alaska (USA). *Ecological Applications*, *23*(8), 1798–1816. <https://doi.org/10.1890/11-0875.1>
- Villalba, G., Whelan, M., Montzka, S. A., Cameron-Smith, P. J., Fischer, M., Zumkehr, A. T., et al. (2021). Exploring the potential of using carbonyl sulfide to track the urban biosphere signal. *Journal of Geophysical Research: Atmospheres*, *126*(13), e2020JD034106. <https://doi.org/10.1029/2020JD034106>
- Wang, Y., Deutscher, N. M., Palm, M., Warneke, T., Notholt, J., Baker, I., et al. (2016). Towards understanding the variability in biospheric CO<sub>2</sub> fluxes: Using FTIR spectrometry and a chemical transport model to investigate the sources and sinks of carbonyl sulfide and its link to CO<sub>2</sub>. *Atmospheric Chemistry and Physics*, *16*(4), 2123–2138. <https://doi.org/10.5194/acp-16-2123-2016>
- Wehr, R., Commane, R., Munger, J. W., McManus, J. B., Nelson, D. D., Zahniser, M. S., et al. (2017). Dynamics of canopy stomatal conductance, transpiration, and evaporation in a temperate deciduous forest, validated by carbonyl sulfide uptake. *Biogeosciences*, *14*(2), 389–401. <https://doi.org/10.5194/bg-14-389-2017>
- Whelan, M. E., Anderegg, L. D. L., Badgley, G., Campbell, J. E., Commane, R., Frankenberg, C., et al. (2020). Scientific communities striving for a common cause: Innovations in carbon cycle science. *Bulletin of the American Meteorological Society*, *101*(9), E1537–E1543. <https://doi.org/10.1175/bams-d-19-0306.1>
- Whelan, M. E., Lennartz, S. T., Gimeno, T. E., Wehr, R., Wohlfahrt, G., Wang, Y., et al. (2018). Reviews and syntheses: Carbonyl sulfide as a multi-scale tracer for carbon and water cycles. *Biogeosciences*, *15*(12), 3625–3657. <https://doi.org/10.5194/bg-15-3625-2018>
- Zona, D., Gioli, B., Commane, R., Lindsaas, J., Wofsy, S. C., Miller, C. E., et al. (2016). Cold season emissions dominate the Arctic tundra methane budget. *Proceedings of the National Academy of Sciences*, *113*(1), 40–45. <https://doi.org/10.1073/pnas.1516017113>